The influence of train traffic on rock slope stability: A dynamic approach

Albena Peycheva Dimitrova

Thesis to obtain the Master of Science Degree in

Mining and Geological Engineering

Supervisor:

Professor Gustavo André Paneiro

Examination Committee

Chairperson: Prof. Jose Manuel Vaz Velho Barbosa Marques

Supervisor: Prof. Gustavo André Paneiro

Member of the Committee: Prof. Maria Amélia Alves Rangel Dionísio

October 2021

Dedicated to my father

Declaration

I declare this document is an original work of my own and that it fulfills all the requirements of the Code of Conduct and Good Practices of the Universidade de Lisboa.

Acknowledgements

I would like to thank to my advisor, Professor Gustavo Paneiro, for introducing me to the topic of slope stability with dynamic loading and for giving me the opportunity to develop the work presented here. I would also like to express my thanks for all the guidance and help throughout this thesis.

I am very thankful to the program “Erasmus+” for giving me the opportunity to work on this thesis in Instituto Superior Tecnico, Lisbon with the cooperation of my home university – University of Mining and Geology “Saint Ivan Rilski”, Sofia.

I would also like to thank my family and friends for their patience and support.

Abstract

Bulgaria has a strategic geoeconomical location, as it has the only railway connecting the European Union and Turkey. In the last years railways are being renewed, so they could allow higher speed of the trains. However, the rails are designed for higher speeds than the trains can reach. With the future replacement of the older trains with new faster ones, problem of stability of the nearby slopes that have not been subjected to the vibrations of trains with the new higher speeds will arise.

Analyzing the problem of stability of rock slopes in the railway line of Beira Alta (Portugal) after modernization is a case study on which it can be examined how trains influence the stability of the nearby slopes. The region of the chosen slope is built of weathered fractured coarse-grained granites.

The present work aims to discuss and compare results of slope stability analysis using various methods. Static stability analysis is made using kinematic method of Markland performed with application *Dips*, limit equilibrium method formulas and program *SWedge*. Finite element method (FEM) is applied to static and dynamic analysis with software *RS2* from *Rocscience* for 2-dimensional modelling. The dynamic analysis includes modelling the railway-induced ground vibrations and constructing a trench as a mitigation measure.

The work suggests comparison between the different methods used for estimating the static safety factor. The dynamic analysis performed shows that there is an influence of the rock slope stability when a dynamic loading of a train-induced ground vibration is introduced. The mitigation measure of an open trench reduces the ground vibrations up to 30% in horizontal and up to 40% in vertical direction.

Keywords: rock slope stability; railway-induced ground vibration; safety factor; static analysis; dynamic analysis; ground vibration mitigation; kinematic method of Markland; limit equilibrium method; FEM

Resumo

A Bulgária tem uma localização estratégica, pois possui a única ferrovia que liga a União Europeia à Turquia. Nos últimos anos, a intensa renovação das ferrovias permite maior velocidade de circulação das composições. Como resultado, poderão surgir problemas de estabilidade dos taludes próximos das ferrovias, os quais ficarão sujeitos a maiores solicitações dinâmicas resultantes da circulação das composições ferroviárias a maior velocidade. A análise do problema de estabilidade dos taludes rochosos da linha férrea da Beira Alta é um estudo de caso no qual se pode examinar como os comboios influenciam a estabilidade dos taludes próximos.

O presente trabalho tem como objetivo discutir e comparar resultados de análises de estabilidade de taludes utilizando o método cinemático de Markland, fórmulas do método de equilíbrio limite e o programa SWedge para análise estática. O método dos elementos finitos é aplicado à análise estática e dinâmica com o software RS2 (Rocscience). A análise dinâmica inclui a modelação das vibrações nos terrenos induzidas pelo tráfego ferroviário e a construção de uma trincheira como medida de mitigação.

O trabalho sugere a comparação entre os diferentes métodos usados para estimar o fator de segurança estático. A análise dinâmica mostra que há uma influência da estabilidade do talude da rocha quando uma solicitação dinâmica induzida pela circulação de composições ferroviárias é considerada. A medida de mitigação de uma trincheira aberta reduz as vibrações do solo em até 30% na direção horizontal e até 40% na direção vertical.

Palavras-chave: estabilidade de taludes de rocha; vibração do solo induzida por ferrovia; factor de segurança; análise estática; análise dinâmica; mitigação de vibração do solo; método cinemático de Markland; método do equilíbrio limite; FEM

Table of contents

List of Figures

List of Tables

List of Equations

1. Introduction

1.1. Motivation

Bulgaria has a strategic geoeconomical location, as it has the only railway connecting the European union and Turkey. The European Environment Agency (EEA) report term 2014 – Annex 6 shows that the railway transport produces the least CO_2 emissions per passenger per km. The rail transport is indicated to be the best performer in terms of environmental impact. As such, this mode of long-distance transportation is worth investing into.

In the last years railways are being renewed with perspective to track renovation, so they could allow higher circulation speed. According to the description of the project in Operational Program Transport and Transport Infrastructure (OPTTI 2014-2020), after modernization the railways will allow maximum speed of 160 km/h for passenger trains and 120 km/h for freight trains. The most widely used locomotives in Bulgaria are Locomotive series 41.000-46.000 and series 06.000-07.000 (Figure 1.1a) (Деянов, 1993), with maximum speeds of 70 km/h and 100 km/h, respectively. Since 2019 the Siemens Smartron locomotive (Figure 1.1b) is put into use which can reach 160 km/h. With the replacement of the older trains with new faster trains in the future, stability problems may arise in railway section with nearby rock slopes that have not been subjected to the vibrations of trains with higher speeds.

a.

b.

Figure 1.1: a – Locomotive series 07.00; b – Locomotive Siemens Smartron (Bulgarian National Railways - BDZ).

Analyzing the problem of stability of rock slopes in the railway line of Beira Alta (Portugal) is a case study on which it can be examined how trains influence the stability of the nearby slopes.

The survey includes static and dynamic analysis of rock slope stability, which could be applied in any case of rock slope – excavations or natural slopes. The dynamic analysis includes dynamic loading induced by a train passing nearby.

The slope considered in this work is chosen to be with the lowest safety factor among those analysed in the previous work of Costa (2019). This study suggests additional evaluation of the influence of the train composition passage with a trench, near the train track, working as a barrier to ground vibration propagation due to train traffic.

1.2. Goals

The present work aims to discuss and compare results of slope stability analysis using various methods. Static stability analysis of the chosen slope, prone to sliding, is made using kinematic method of Markland performed with application *Dips*, limit equilibrium method formulas and the software *SWedge*. Finite element method (FEM) is applied to static and dynamic analysis with software *RS2* from *Rocscience* for 2-dimensional modeling with a different approach to building the model.

Understanding the influence of a train on ground vibration propagation requires studying the train composition, the distribution of the loading on the embankment and the bed rock. The next step would be to create a model that simulates the dynamic load as realistic as possible.

A comparison between the different methods is made and the results from the dynamic analysis show whether the passing of a train influences the stability of the nearby rock slope. The differences in methodology and the results between the current study and Costa (2019) are discussed. Another goal this work aims to obtain is to show how a trench between the railway track and the slope would prevent the vibrations induced by train traffic to reach the slope and influence the slope stability.

1.3. Organization

This dissertation is divided into six chapters, the first containing a short introduction to the work to be developed and the areas of interest, as well as the goals to be achieved and its organization.

The second chapter presents the theoretical view on the studied problem, specifically about ground vibrations generation and propagation. In the third chapter, reference is made to the case study, with general description, geological setting, seismicity of the region, characterization of the slope, geomechanical parameters of the intact rock and the rock mass, as well as data concerning the dynamic aspect of the physical process. In the fourth chapter, the methodology used is shortly

presented. In the fifth chapter, the results from the analyzes carried out using the various methods are presented and discussed.

Finally, in the sixth chapter, conclusions of the work are presented and reference is made to the work that may be developed in this area of study in the future.

2. Bibliographic review

2.1. Ground vibrations generation by train traffic

Vibrations usually arise at the contact of the moving train wheel with the rail (Connolly et al., 2015). Then they are transmitted through the railway track and to the ground. There they spread in the form of stress waves. In the involved physical phenomena, 4 types of waves – primary (P-waves), secondary (S-waves), Rayleigh waves and Love waves – are usually considered. Primary waves are also known as compression waves because they generate movements of compression and dilation. Secondary waves are known as shear waves as they deform the propagation media according to movement perpendicular to the wave spread direction. They have lower propagation velocity than the primary waves. Primary and secondary waves are defined as body waves. Surface waves are two types – Love and Rayleigh waves. Figure 2.1 shows the spreading of the different waves types. An emphasis is placed on the propagation of Rayleigh waves as they transmit approximately two thirds of the total excitation energy (Rayleigh waves - 67%, S-waves - 26%, P-waves - 7%) (Miller and Pursey, 1955).

According to Rayleigh (1885) in Rayleigh waves the particle velocity is perpendicular to the direction of the wave propagation, and propagates in elliptical motion. Because these waves spread only into two dimensions, their attenuation is poor (Rayleigh, 1885). The Rayleigh waves are active only in a thin layer at the surface, so their energy density is large which leads to exhibition of very large amplitudes (Rayleigh, 1885). The wave amplitude diminishes exponentially with increasing distance from the surface (Rayleigh, 1885). Due to the weak attenuation of these waves, in seismics the surface waves at larger distances are dominant and are responsible for the resulting damage (Rayleigh, 1885).

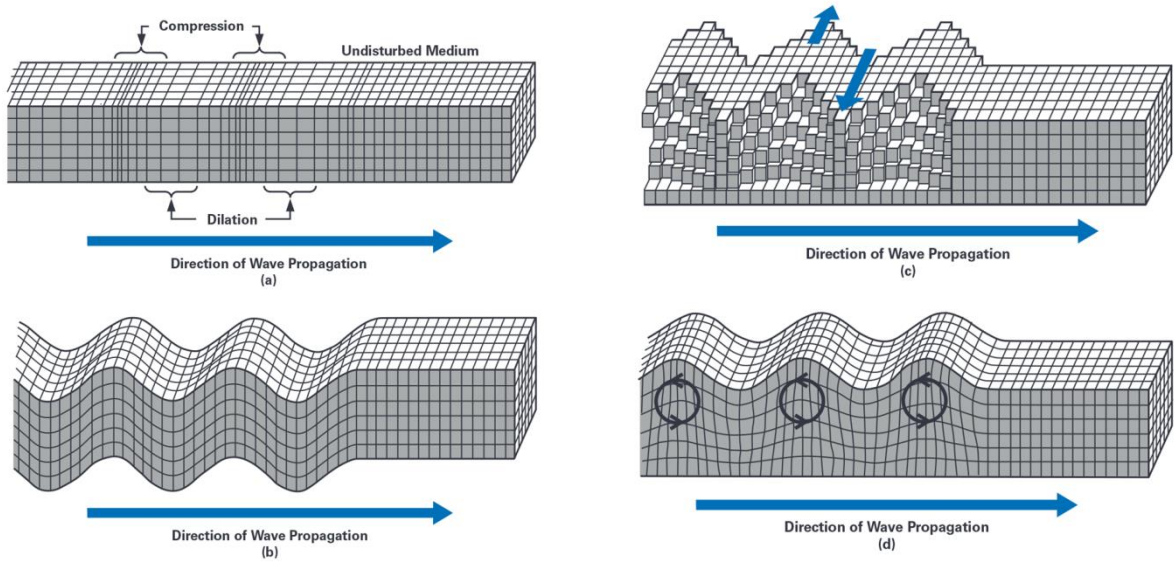

Figure 2.1: Seismic waves propagation: a – primary waves; b – secondary waves; c – Love waves; d – Rayleigh waves (image adapted from Olivadoti, 2001).

The railway track is constructed of rails with rail pads, which lie on concrete or wood sleepers, which are set on a ballast embankment. The layer underlying the ballast is called the subballast. Subballast layers are not always utilized in track construction (Wang, 2016). All this structure lays on the subgrade, which is the natural soil or rock formation. A typical cross-section of a railway track is shown on Figure 2.2. The functions of ballast include (Wang, 2016):

- transfer of the imposed loadings uniformly to the subgrade soil (roadbed) at a stress tolerable for the particular material in the roadbed;
- provide uniform support for the ties with the necessary degree of elasticity and resilience to absorb vibrations and shock;
- anchor the track in place and resist vertical, lateral, and longitudinal movements;
- provide immediate free drainage and prevent the growth of vegetation;
- resist aggregate degradation due to physical forces exerted by traffic and maintenance equipment and environmental factors such as freeze-thaw and wet-dry.

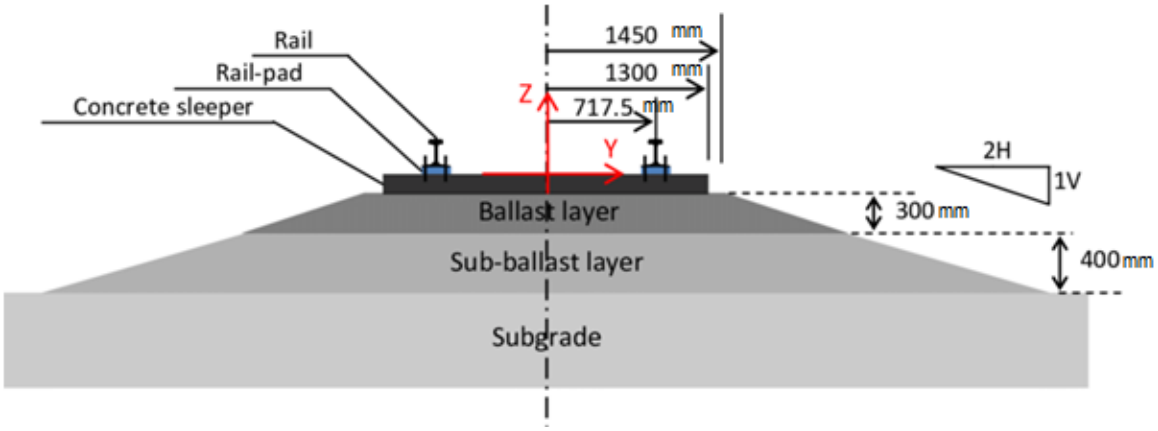

Figure 2.2: Typical cross-section of a railway track (Mezeh, 2017).

Figure 2.3 shows a schematic representation of a general track model presented by Connolly et al (2015). The parts of the superstructure bogies and wheels are connected with primary suspension which is characterized by damping and stiffness. The secondary suspension lays between the car and the bogies. Schematically the parts of the substructure – sleepers, ballast and subgrade – are also connected by a damper and a spring rheological model. The spring represents the stiffness properties and the damper the damping properties of the material.

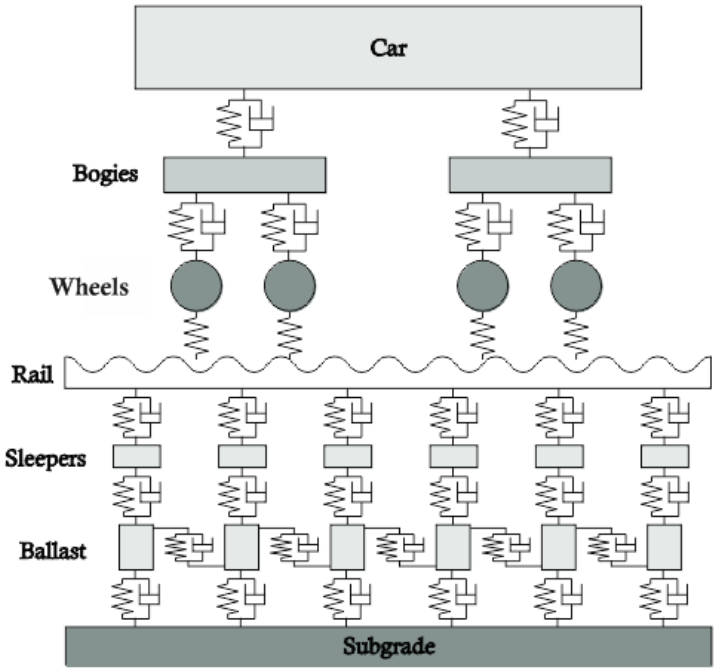

Figure 2.3: Simplified schematic representation of the rheological model of train circulation in a railway track (Connolly et al., 2015).

The vibrations induced by the train circulation depend on many factors and some of the main ones are the condition of the rails and wheels and the primary suspension which is the springs and dampers connecting the bogies to the wheels (Connolly et al., 2015). The more rigid the suspension, the more vibrations will be produced (Connolly et al., 2015). Considering the wheels, imperfections such as wheel out-of-roundness and wheel corrugation can provoke vibrations (Connolly et al., 2015). Referring to the rails, rail corrugation is the main factor for ground vibrations production (Connolly et al., 2015).

When ground vibrations are produced they travel through the railway embankment and the ground reaching nearby structures, buildings or slopes. The way the vibration will affect them depends on ballast bed with its damping properties and the type of soil that the geological strata is built up of (Connolly et al., 2015). The ballast embankment with its damping effect, attenuates part of the energy of the induced seismic wave, so ground vibrations will be partly absorbed by the time they reach the natural subgrade. In terms of the ground type, in clayey types of soils vibrations have higher impact compared to sand (Dinis da Gama and Paneiro, 2006).

2.2. Damping

Attenuation (or damping) is a measure of the rate at which energy is reduced in a time or space interval. Damping is usually greater in the upper part of the geological profile and reduces with depth

(Connolly et al., 2015). This is because the soil particles in the upper layers are less compacted, meaning the wave loses greater energy as it passes through the air voids (Connolly et al., 2015). On the other hand, damping in rocks is much smaller compared to damping in soils.

Zerwer et al. (2002) discussed the Rayleigh damping model which is used in this study. In dynamic finite element analysis, the leading equation of motion when the system is subjected to external forces is expressed as (Caughey, 1960):

$$[M]\{\ddot{u}\} + [C]\{\acute{u}\} + [K]\{u\} = \{F\} \qquad \text{Equation (1)}$$

where ü, ú and u represent the acceleration, velocity and displacement, respectively. The mass matrix is given by M, the damping matrix is C, and the stiffness matrix is K. Caughey (1960) showed that the damping matrix could be expressed as a linear combination of the mass and stiffness matrices. This type of damping is referred to as Rayleigh damping. Liu and Gorman (1995) gave the final standard Rayleigh damping equation:

$$[C] = \alpha\,[M] + \beta\,[K] \qquad \text{Equation (2)}$$

where α and β are respectively the mass and the stiffness damping coefficients. Their relationship with the damping ratio is the following (Figure 2.4) (Rocscience, 2020):

$$\zeta = \frac{\alpha_M}{2\omega_n} + \frac{\beta_K \omega_n}{2} \qquad \text{Equation (3)}$$

where ζ is the damping ratio and ω is the natural (or ressoant) frequency of the system. To calculate the Rayleigh damping coefficients, two typical frequencies are chosen and the values are obtained as follows (Rocscience, 2020):

$$\alpha_M = \zeta \frac{2\omega_1\omega_2}{\omega_1+\omega_2} \qquad \text{Equation (4)}$$

$$\beta_K = \zeta \frac{2}{\omega_1+\omega_2} \qquad \text{Equation (5)}$$

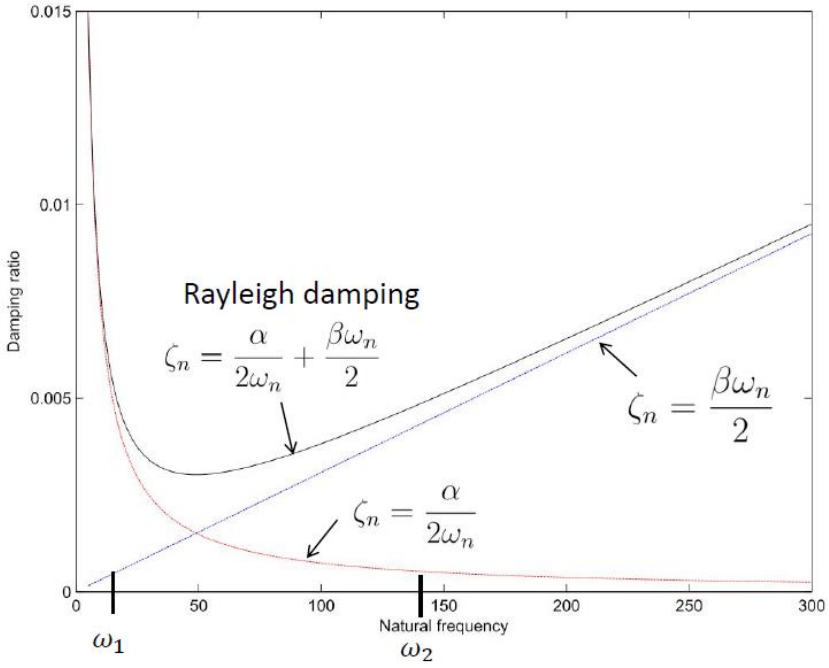

Figure 2.4: Rayleigh damping: Natural frequency vs. Damping ratio graph (Rehnström and Widén, 2012). ω_1 and ω_2 are two chosen frequencies used to calculate the Rayleigh damping coefficients.

Anbazhagan and Parihar (2015) made a study on the damping curves for different types of soils. In the current study, for the embankment made of ballast, the proper damping ratio is chosen according to the damping curve for sand on Figure 2.5 (Seed and Idriss,1970). Rollins (1998) made a study over data of cyclic shear tests performed on gravels to determine shear modulus and damping relationships. According to this study, the mean curve for gravels is close to the curve for sand determined by Seed and Idriss (1970). The damping ratio curve developed by Schnabel et al. (1973) is used for rocks (Figure 2.6).

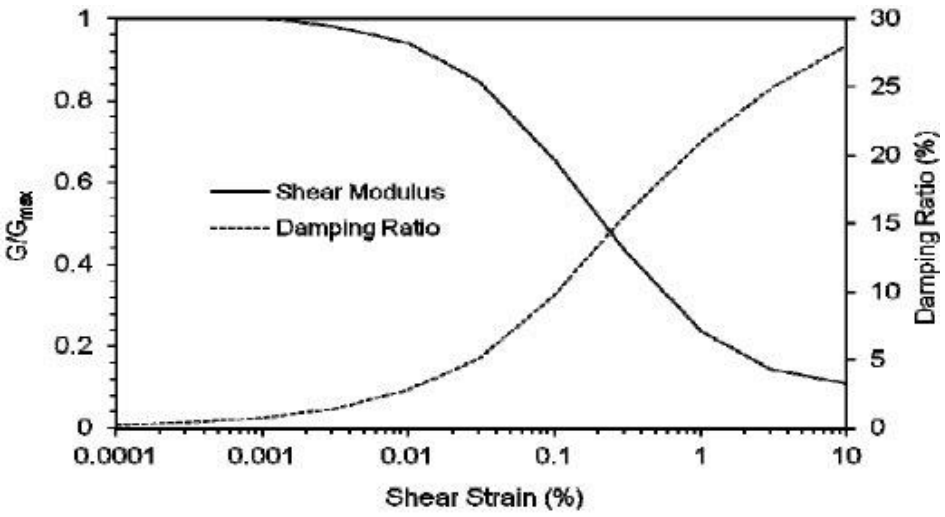

Figure 2.5: Damping curve for sand. (Seed and Idriss, 1970)

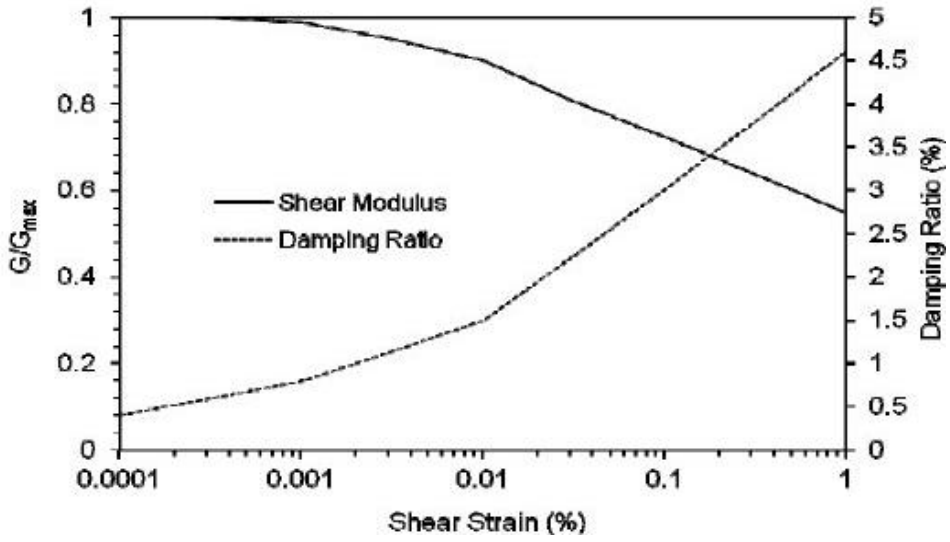

Figure 2.6: Damping curve for rock. (Schnabel et al., 1973)

2.3. Ground vibrations mitigation

There are different measures that could be taken to limit ground vibrations induced by train traffic, so that the impact on nearby structures, buildings and slopes is minimized. Some of these measures include placing damping mats, buried walls, trenches, etc. (Paul de Vos, 2017). The measure that this work is focused on is the trench. Research on this ground vibration mitigation measure was made by Woods (1968), Dinis da Gama and Paneiro (2006), Alzawi and Hesahm El Naggar (2010), Cęlebi and Kirtel (2013). Woods (1968) made field tests with a circular and partial circular trenches around the surface source of ground vibrations. The propagation medium is silty sand and sandy silt. The results show a decrease in amplitude by up to 87%. Woods (1968) suggested that the minimum trench depth should be $0.6\lambda_r$ for active isolation and $1.33\,\lambda_r$ for passive isolation to obtain an average reduction of 75% in vertical ground vibration, where λ_r is the Rayleigh wave length.

Dinis da Gama and Paneiro (2006) carried out analyzes to obtain the vibration speed caused by the circulation of a light railway composition in a tunnel in sandy ground and in clayey ground (Figure 2.7). To minimize the ground vibrations induced by the passage of a train in an underground railway line, lateral voids near the light railway track were considered (Figure 2.8). The comparison between the case without the existence of lateral trenches and the case with the existence of them shows that in a surface building the vibrations' velocity is reduced by 48.5% for sandy materials and 55.6% for clayey materials. According to the author, this phenomenon is due to the complex mechanisms of reflection and refraction caused by the existence of voids. The presence of lateral holes limits the propagation of vibrations near the source and directs them downwards.

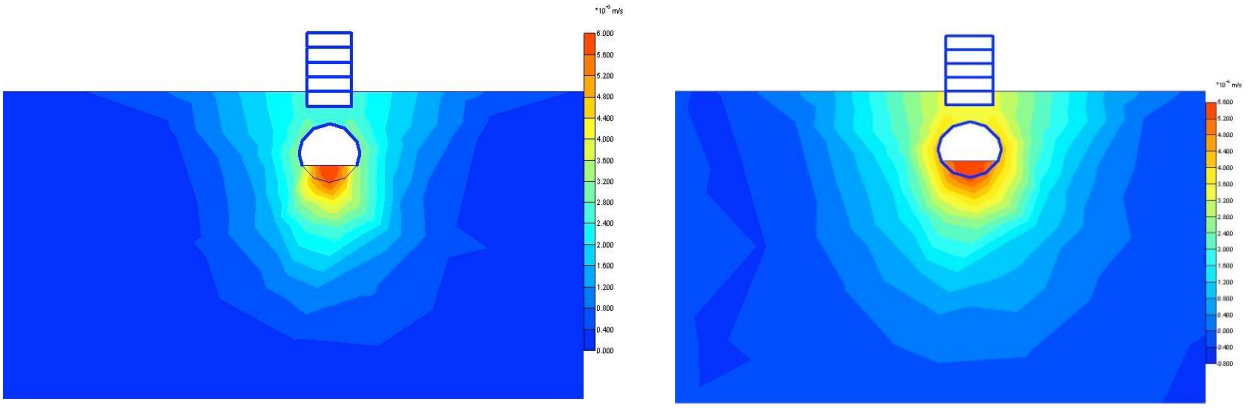

Figure 2.7: Initial situation of vibration velocities in sandy (left) and clayey (right) soils. (Dinis da Gama and Paneiro, 2006)

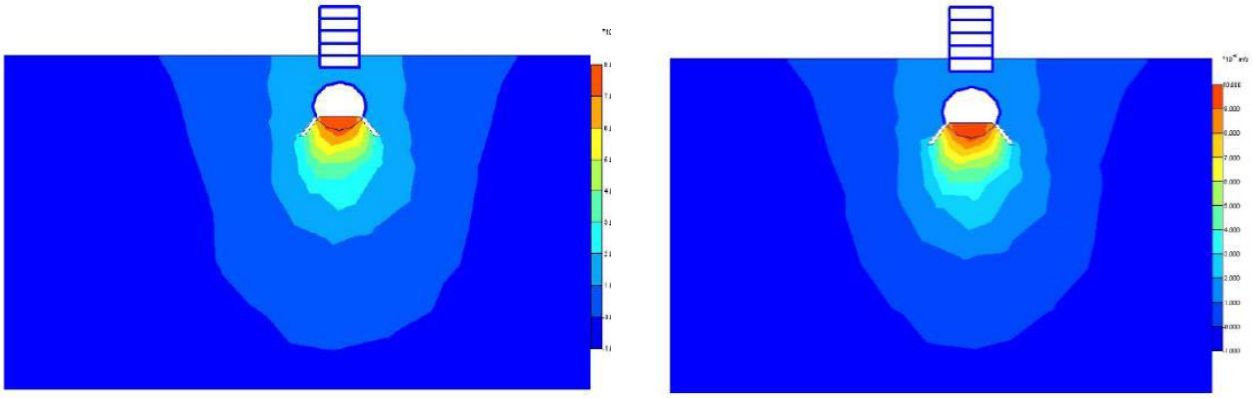

Figure 2.8: Vibration velocity variation in sandy (left) and clayey (right) soils, considering two cavities in the track, near the origin of the dynamic forces caused by train traffic. (Dinis da Gama and Paneiro, 2006)

Çelebi and Kirtel (2013) simulated wave propagation, considering the effect of the passage of railway compositions on a railway, running at different speeds, applying a two-dimensional finite element model with the Mohr-Coulomb approach. This work aimed to study the implementation of trench barriers to isolate foundations and structures from vibrations induced by surface rail traffic (Figure 2.9). This type of trench is applied in the current survey to limit the vibrations to reach the slope.

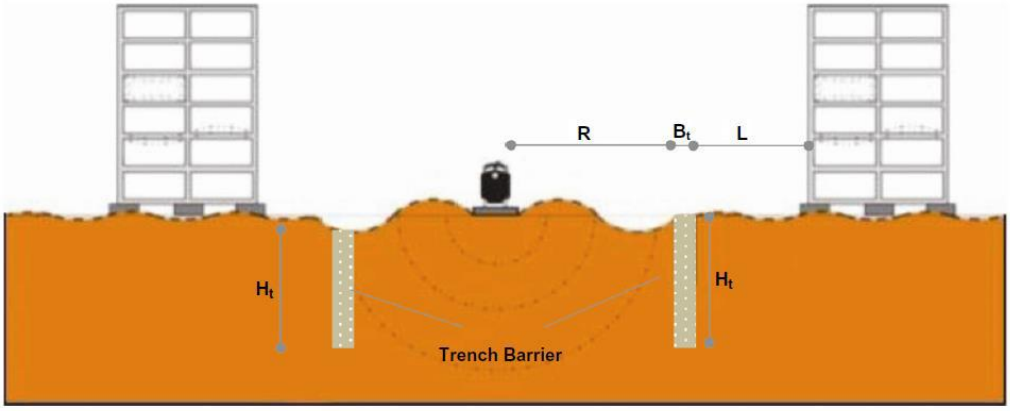

Figure 2.9: Reduction of vibrations induced by rail traffic through the implementation of filled ditch barriers (Cęlebi and Kirtel, 2013) where R is the distance between the vibration producer and the barrier, L – distance between the barrier and the building where the influence of the vibrations is observed; B_t – width of the trench, H_t – hight of the trench.

After analyzes carried out before and after the construction of the isolation barrier, it is concluded that (Cęlebi and Kirtel, 2013):

- Open trenches with depths of 4.5 meters have significant effects in attenuating the structural response, verifying a reduction of up to 85% of vertical vibrations;
- The most efficient vibration method is to place an open trench in the vicinity of the railway line, considered active vibration isolation. The main reduction being obtained when the distance between the vibration source and the screen is 5 meters;
- The distance from the buildings to the wave barrier has no effect on reducing vertical vibrations, on the contrary, a significant part of the surface waves is reflected on the front face of the screen and can amplify the vibration levels;
- The influence of train speed on the structure response is related to the mechanical properties of the terrain.

The physical explanation of how the trench reduces vibrations is due to the impedance difference of the two materials – rock and air. The difference in acoustic impedance between materials leads to reflection of the seismic wave. The ratio of amplitude of the reflected wave to the incident wave, or how much energy is reflected. From the geophysics if the wave has normal incidence, then its reflection coefficient can be expressed as (Lines and Vasheghani, 2008):

$$R = (\rho_2 V_2 - \rho_1 V_1) / (\rho_2 V_2 + \rho_1 V_1), \quad \text{(Equation 6)}$$

where

R – reflection coefficient, whose values range from −1 to +1;

ρ1 – density of medium 1;

ρ2 – density of medium 2;

V1 – stress wave propagation velocity of medium 1;
V2 – stress wave propagation velocity of medium 2.

The quantity ρV is the seismic impedance of the material. The Reflection Coefficient is therefore the difference in seismic impedance over the sum of seismic impedance of two materials. From the above equation, it is apparent that R will be a positive number when $V_2 > V_1$, and a negative number when $V_2 < V_1$ (Geometrics, 2018). Typical values of R are approximately −1 from water to air, meaning that nearly 100% of the energy is reflected and none is transmitted. If R is approximately 1, nearly all the energy is transmitted and none is reflected. It should also be apparent that the larger the contrast in seismic impedance, the larger the amount of incident energy that is reflected (and the smaller the amount that is transmitted) (Geometrics, 2018).

3. Case study

3.1. Location

The slope considered on this study is located on the railway line of Beira Alta in the north of Portugal, in the section between Mangualde and Guarda as shown on Figure 3.1. The slope is on the East side of the track from km 194+180 to km 194+400. The examined area is about 11 km north from Guarda, 8 km South from Vila Franca das Naves, 2.5 km East from Velosa. Approximate coordinates are:

- Latitude: 40°39'22" N
- Longitude: 7°15'49" W
- Altitude: 680 m.a.s.l.

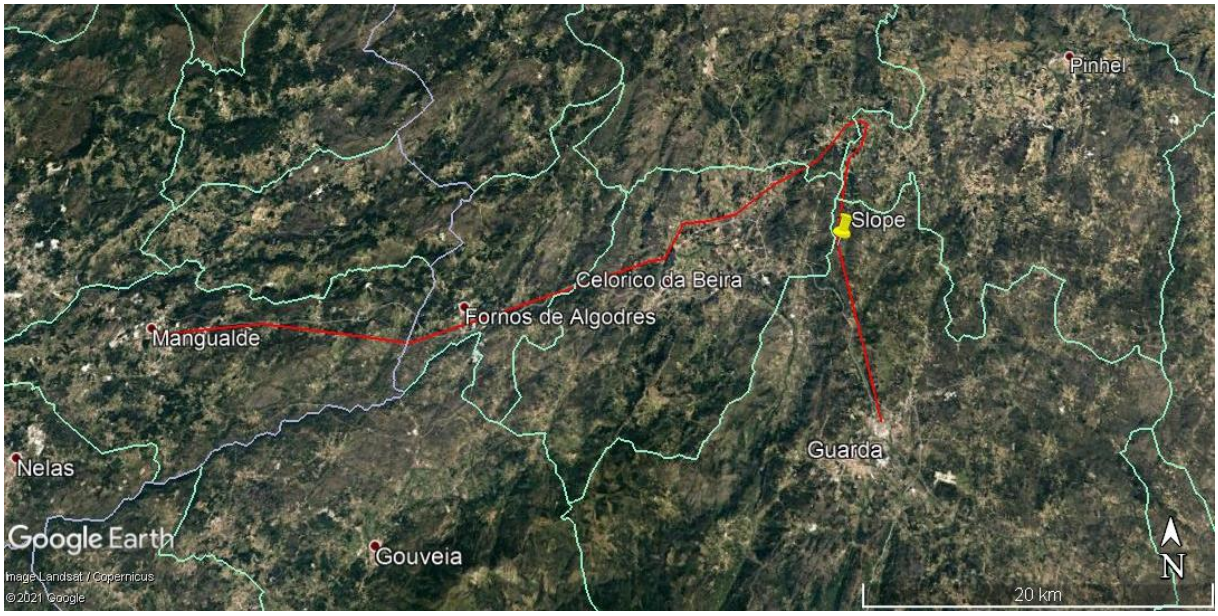

Figure 3.1: Location of the slope (yellow pin) on the railway line between Mangualde and Guarda (red line). (image – Landsat / Copernicus)

3.2. Geology of the region

The studied area is described in geological map sheet 18-A Vila Franca das Naves of the scale 1:50 000. The region is a part of the Central Iberian zone of the Iberian Massif, which is a result of paleozoic orogenic activity (Neves Ferro et al., 1962). The rocks found here are very fractured monzonitic granites ($\gamma\pi_g$), very coarse-grained, often porphyry (Neves Ferro et al., 1962). The rock is with bluish tone on fresh surface, dominating porphyroid facies with large crystals of feldspar (Neves Ferro et al., 1962). In the region there are veins of basic rocks, often dolerite dikes embedded in the granite, which is crushed at the contact with the veins (Neves Ferro et al., 1962). Their main orientation is north-south. Sometimes they interlock with quartz veins (Neves Ferro et al., 1962).

The most important regional tectonic structure is the Bragança-Vilariça-Manteigas fault zone with orientation NNE-SSW (Neves Ferro et al., 1962).

The relief is hilly. The main physico-geological processes that occur are erosion and rockfalls. The region covered by the map of Vila Franca das Naves belongs largely on the extensive erosion surface of the Meseta (Neves Ferro et al., 1962). The current morphology of the region is the result of different actions, in which erosion phenomena stands out (Neves Ferro et al., 1962).

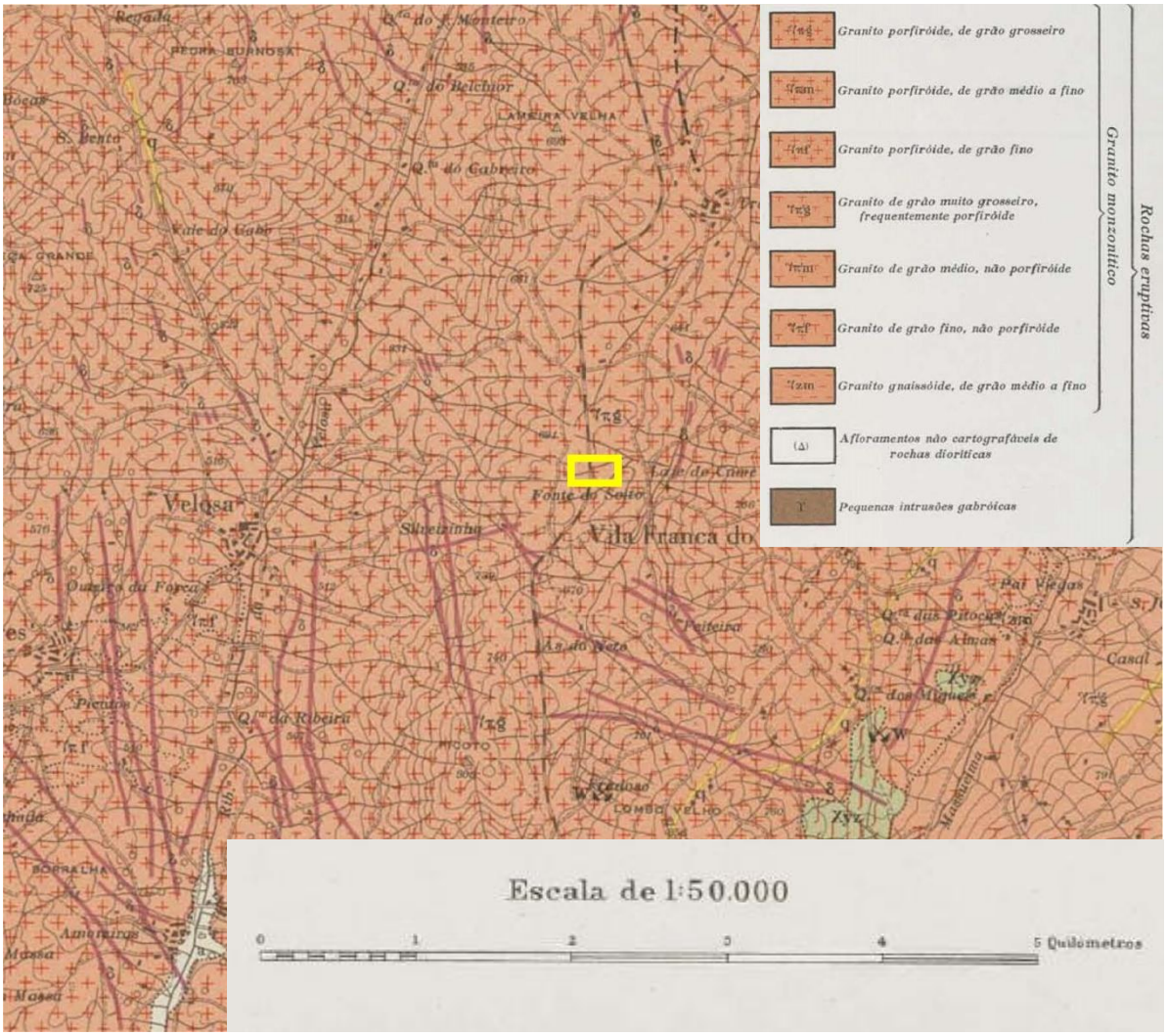

Figure 3.2: Geological map of the region with a scale 1:50 000. The slope is located in the yellow rectangle. (Laboratório Nacional de Energia e Geologia)

3.3. Description of the slope

The slope is made up of weathered fractured coarse-grained granites. The slope is 220 m long with a maximum height of 15 m. There is little vegetation (Figure 3.3). There are five groups of joints found in the rock mass. The slope face has a dip direction and dip of 119° and 54° respectively. Accoring to the

ISRM (International Society of Rock Mechanics) weathering grade classification (Table 1), the rock mass has a grade III of weathering – moderately weathered (MW).

Table 1: Weathering grades of rock mass (ISRM, 1981a)

Term	Symbol	Description	Grade
Fresh	F	No visible sign of rock material weathering; perhaps slight discolouration on major discontinuity surfaces.	I
Slightly weathered	SW	Discolouration indicates weathering of rock material and discontinuity may be somewhat weaker externally than in its fresh condition.	II
Moderately weathered	MW	Less than half of the rock material is decomposed and/or disintegrated to a soil. Fresh or discoloured rock is present either as a continuous framework or as a corestones.	III
Highly weathered	HW	More than half of the rock material is decomposed and/or disintegrated to a soil. Fresh or discoloured rock is present either as a discontinuous framework or as a corestones.	IV
Completely weathered	CW	All rock material is decomposed and/or disintegrated to a soil. The original mass structure is still largely intact.	V
Residual soil	RS	All rock material is converted to a soil. The mass structure and material fabric are destroyed. There is a large change in volume, but the soil has not been significantly transported	VI

Figure 3.3: Photo of the slope (Costa, 2019).

3.3.1. Geotechnical parameters of the intact rock

The properties of the rock material have been adapted from a previous study on these rocks (Costa, 2019). They had been obtained through laboratory tests and treated statistically, therefore being characteristic values (Costa, 2019). They are shown in Table 2.

Table 2: Properties of the rock.

Property	Value
Unit weight ɣ	26 kN/m^3
Porosity n	0.12
Uniaxial compressive strength C_0	106 MPa
Cohesion c	21.2 MPa
Internal friction angle φ	51°
Poisson's ratio v	0.2
Young's modulus E	32 000 MPa

Due to lack of data required for the examination of the problem, some of the properties have been obtained from surveys and tables with typical values for weathered granite. The failure criterion used in this study is the Mohr-Coulomb criterion. The shear strength parameters internal friction angle and cohesion have been taken from typical values for granites (Shwartz, 1964). Poisson's ratio has been adapted from (Ji et al., 2018) and (Vàsàrhelyi, 2008). Villeneuve et al. (2018) made research on weathered porphyritic granites and suggested that the Young's modulus E to be estimated using the following formula (Hoek and Diederichs, 2006):

$$E = MR.C_0 \qquad \text{Equation (7)}$$

where MR is a lithology specific factor, which for granite is 300 – 550 (Hoek and Diederichs, 2006). For compressive strength C_0 = 106 MPa this would give a range of E = 31.8 – 58.3 GPa. The chosen value is E = 32 GPa due to the fact that the granite is very weathered.

3.3.2. Geotechnical parameters of the rock mass

The parameters of the rock mass are important to obtain, considering that the main reason for instabilities are the discontinuities. The fractures' system is consisted of intersecting groups of joints that form blocks prone to sliding, falling or toppling.

The discontinuities had been observed for their orientation, persistence and roughness of the surfaces (Costa, 2019). The joints are examined to be with no filling, so the properties will depend only on the rock surface (Costa, 2019). The basic friction angle had been considered taking into account the values suggested by Hoek & Bray (1981) for dry coarse-grained granite and porphyry. Joint Compression Strength (JCS) had been obtained using the Schmidt hammer. The rebound resistance

had been estimated according to the criteria defined by Barton and Choubey (1977). The length of the discontinuities varies in the interval 5-10 m. The Joint Roughness Coefficient (JRC) had been estimated in the interval 7-11 and then corrected for the persistence of the fractures according to (Bandis et al, 1981). With all this data, the friction angle of the discontinuity had been determined according to Barton's failure criterion. The values are shown in Table 3.

Table 3: Properties of the rock mass. (Costa, 2019)

Property	Value
JRC	7 - 11
Length of the fractures L_{joint}	5-10 m
Basic friction angle φ_b	31° - 35°
Overburden (weight of the block)	11 - 520 kPa
Joint friction angle φ_j	38° - 41°

The basic friction angle is chosen to be 31° since the basic friction angle for dry porphyry is 31° and the rocks are described as sometimes such (Neves Ferro et al., 1962) . The overburden is calculated from the geometry of the slope and the unit weight of the rock. The joint friction angle is calculated by the shear strength criterion of Barton from data for several outcrops in the region and the final value chosen to work with is 40° (Costa, 2019).

3.3.3. Joint system

There are five groups of joints found in the examined slope. Their orientation as shown on Table 4. All groups of joints are of equal importance and none of them is indicated as leading. Their properties are similar and the friction angle of the surface of the joints is calculated to be 40°.

Table 4: Joint groups orientation. (Costa, 2019)

Joint group	Dip direction	Dip
J1	192	83
J2	241	83
J3	162	41
J4	210	17
J5	108	87

The orientation of the slope face has dip direction and dip 119°/54°.

3.4. Railway embankment properties

The embankment is built up of ballast with a thickness of 70 cm. The geometry of it is shown on Figure 2.2. The values are taken from the previous study (Costa, 2019) and are given in Table 5..

Table 5: Properties of the embankment material. (Costa, 2019)

Property	Value
Unit weight ɣ	22 kN/m^3
Porosity n	0.5
Cohesion c	0 MPa
Internal friction angle φ	30°
Poisson's ratio v	0.3
Young's modulus E	78 MPa

3.5. Train composition

The train structure chosen for this research consists of a locomotive and 20 wagons. The locomotive is a six-axle model Euro 4000 with a standard gauge of 1435 mm (Figure 3.4). The weight of the locomotive is 123 tons, transmitting 204 kN per axle. The wagons are two-axle model Lgnss (22 94 443 3 001/100) (Figure 3.5). The maximum weight of each wagon together with the freight is 44.8 tons, transmitting 223 kN per axle.

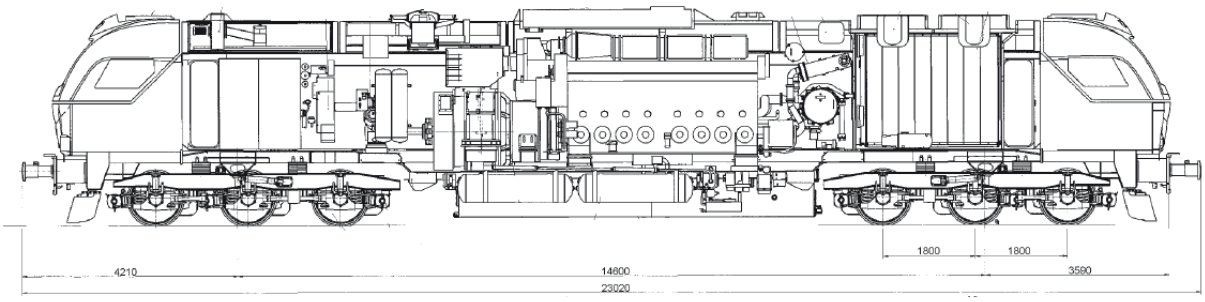

Figure 3.4: Scheme of locomotive Euro 4000 (Medway – Transport and Logistics).

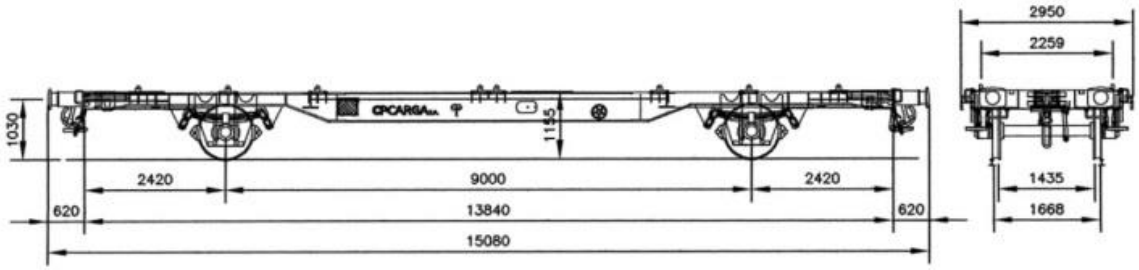

Figure 3.5: Scheme of wagon Lgnss (22 94 443 3 001/100) (CP Carga – Portuguese freight rail operator).

3.6. Induced dynamic load

Train track interaction is a complex process to model (Çelebi, 2012). From a geotechnical point of view, the construction of the train and the track needs to be simplified to work only with the influence of the train passing on the railway embankment and the subgrade. For this work, which is focused on the slope stability, the railway structure is simplified. Usually, the vibrations can be recorded by the means of geophysical methods (Woods, 1968, Göktepe et al., 2014), but for this study a more simple approach is used. The impact from the train passing is presented as a distributed load vs. time graph applied on the railway ballast embankment. The sleepers are acting as a distributor of the loads from the rails to the surface of the ballast. The distributed load is applied on the ballast with the width of the sleeper of 2.60 m. Having the distances between the axles of the locomotive and of the wagons and the speed of the train, the load vs. time graph is built (Figure 3.6).

The impact on the natural rock is applied as a vibration velocity vs. time graph, which will be given later on the results chapter.

4. Methodology

The methods used for evaluation of the static and dynamic slope stability will be presented in this chapter. The data collected from the in situ geological survey, carried out in December 2017, including the geotechnical properties of the rock and the rock massif and the description of the discontinuities with their quantitative parameters is used. Several static slope stability analyzes are performed during this work and dynamic slope stability analysis with the influence of vibration induced by a train passing nearby is carried out.

Firstly, a kinematic analysis is carried out using the application *DIPS* of *Rocscience*. It allows to build stereographic projections of planes and poles of the discontinuities of the rock mass and the slope face, adding the friction angle of the joints and assessing possible instability in planar, toppling or wedge sliding blocks with the method of Markland (Markland, 1972). After the critical block is identified by the kinematic analysis, the limit equilibrium method is applied using application *SWedge* to obtain a global factor of safety (FS). The finite element method (FEM) (using two-dimentional application *RS2* of *Rocsciense*) is applied for static condition for comparison to the limit equilibrium method results. The factor of safety is obtained using the Shear Strength Reduction Method. Finally, the 2D FEM is applied for dynamic conditions to understand whether the external factor of a train passing nearby influences the stability of the slope.

As a study that follows the work of Costa (2019), the methods used for evaluation of the slope stability will be compared and the differences explained.

4.1. Kinematic method and method of Markland

The stability of a bedrock-composed slope is often controlled by the geological structure within the bedrock. In such cases, the geometrical relationships between the geological structures and the orientation of the overlying slope determine the kinematic stability of a slope. Kinematic refers to the geometrically possible motion of a body without consideration of the forces involved. Kinematic analysis is concerned with the direction of movement and movement is possible only if the block is not constrained. With respect to slope stability, kinematic analysis generally is used to evaluate whether blocks or masses of rock may move along geological structures and slide out of the face of a slope (Mote et al., 2004).

Kinematic analysis is used in this work to evaluate the possible slip mechanisms of critical blocks which can be planar sliding, wedge sliding or toppling. In the current study a wedge is defined by two intersecting joint planes. The line of intersection usually has a trend almost equal to the dip direction of the slope face. One condition for a wedge failure is that the intersection line dips steeper than the friction angle of the joints. Another main kinematic condition to be satisfied for wedge sliding to occur is that the angle between the the intersection line and the horizontal plane (α) has to be smaller than the angle between the slope face and the horizontal (ψ) (Figure 4.1). The stereonet with the

stereographic projections illustrates the joint planes, slope face and intersection line. The stereonet defines the shape of the wedge, the orientation of the line of intersection and the direction of sliding. This information can be used to assess the potential for the wedge to slide from the cut face. The kinematic analysis does not give a factor of safety, it only gives information about whether there is or not potential of sliding.

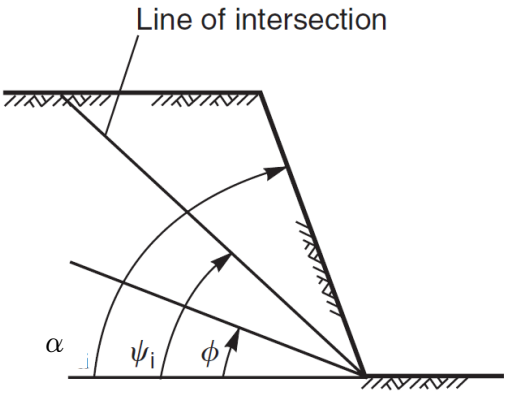

$\alpha > \psi_i$

Figure 4.1: Main kinematic condition for planar slipping. (Wyllie and Mah, 2005)

The method of Markland suggests that a circle of the friction angle is illustrated on the stereonet. Together with the projection of the slope face they interlock the critical area (red hatch zone of Figure 4.2). If the wedge intersection line falls into this area, the wedge is prone to sliding (Figure 4.2).

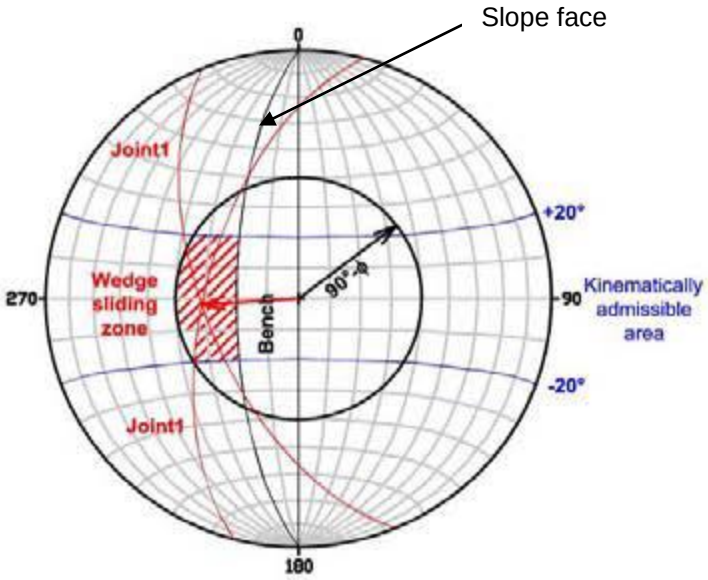

Figure 4.2: Method of Markland – wedge sliding zone (image adapted from Лаков, 2018).

The current study uses the equal-angle stereonet of Wulff.

4.2. Limit equilibrium method

After carrying out the kinematic analysis and having identified the wedges with kinematically admissible global failure mechanisms (wedge failure), the assessment of the global stability under the current conditions is carried out, to assess a factor of safety (FS).

For the calculation of the safety factor of a wedge two different schemes can be used. One of them is to treat the wedge as a planar block with orientation of the sliding surface as of the line of intersection. Therefore, the plunge of the intersection line will be the dip angle of the sliding surface. The forces scheme is shown on Figure 4.3 (c) and the safety factor is the ratio of the resisting forces to the driving forces and is calculated as follows (Wyllie and Mah, 2005) :

$$FS = \frac{W.cos\psi.tg\varphi_{joint}}{W.sin\psi} = \frac{tg\varphi_{joint}}{tg\psi} \qquad \text{Equation (8)}$$

where W is the weight of the wedge, ψ is the inclination of the line of intersection and φ_{joint} is the friction angle of the line of intersection (of the joints).

The second scheme is to calculate the safety factor for the wedge with its geometry in 3 dimensions and properties of each joint plane (Figure 4.3). Assuming that sliding is resisted only by friction and that the friction angle φ_{joint} is the same for both planes, the safety factor is given by (Wyllie and Mah, 2005):

$$FS = \frac{(R_A+R_B).tg\varphi_{joint}}{W.sin\psi} \qquad \text{Equation (9)}$$

where R_A and R_B are the normal reactions provided by planes A and B as illustrated in Figure 4.3, ψ_i is the plunge of the intersection line (Wyllie and Mah, 2005).

$$R_A + R_B = \frac{W.cos\psi.sin\beta}{\sin(\frac{\zeta}{2})} \qquad \text{Equation (10)}$$

where β and ζ are measured as shown on Figure 4.3 (b). Therefore, from equations (9) and (10):

$$FS = \frac{sin\beta.tg\varphi_{joint}.tg\psi}{sin(\frac{\zeta}{2})} \qquad \text{Equation (11)}$$

The equation Hoek et al. (1973) suggests estimating the safety factor of a wedge, incorporating the slope geometry, different shear strengths of the two slide planes and ground water, by the following formula (Hoek et al, 1973)):

$$FS = \frac{3}{\gamma_r H}(c_A X + c_B Y) + \left(A - \frac{\gamma_w}{2\gamma_r} X\right).tg\varphi_A + \left(B - \frac{\gamma_w}{2\gamma_r} Y\right) tg\varphi_B \qquad \text{Equation (12)}$$

where c_A and c_B are the cohesive strengths, and φ_A and φ_B are the angles of friction respectively on planes A and B, γ_r is the unit weight of the rock, γ_w is the unit weight of the water, H is the total height of the wedge. The dimensionless factors X, Y, A and B depend upon the geometry of the wedge and are calculated by formulas. A rapid check of the stability of a wedge can be made if the slope is drained and there is zero cohesion on both the slide planes A and B. Under these conditions, equation (12) reduces to (Wyllie and Mah, 2005):

$$FS = A.tg\varphi_A + B\ tg\varphi_B \qquad \text{Equation (13)}$$

The dimensionless factors A and B are found to depend upon the dips and dip directions of the two planes. The values of these two factors have been computed for a range of wedge geometries, and the results are presented as a series of charts (Annex 1). Many trial calculations have shown that a wedge having a factor of safety in excess of 2.0, as obtained from the friction-only stability charts, is unlikely to fail under even the most severe combination of conditions to which the slope is likely to be subjected. Slopes with a factor of safety, based upon friction only, of less than 2.0 must be regarded as potentially unstable and require further detailed examination such as comprehensive wedge analysis (Hoek and Bray, 1981). The equations of comprehensive wedge analysis form the basis of the application of *Rocscience – SWedge*, which is used in this work.

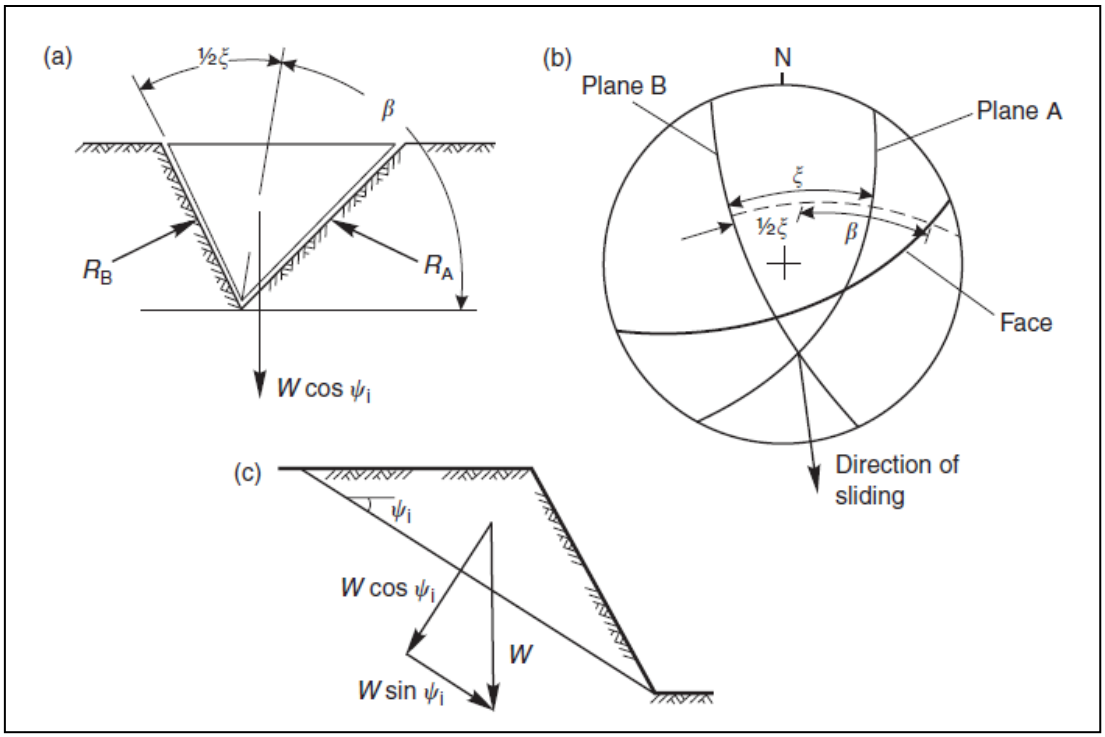

Figure 4.3: Resolution of forces to calculate factor of safety of wedge: (a) view of wedge looking at face showing definition of angles β and ξ, and reactions on sliding planes R_A and R_B; (b) stereonet showing measurement of angles β and ξ; (c) cross-section of wedge showing resolution of wedge weight W. (Wyllie and Mah, 2005)

4.3. Finite element method

The finite element method (FEM) is a continuous numerical modelling method used widely in the engineering practice (Carter, 1996). In general, the method helps analyze a physical problem by creating a model involving three phases (shown on Figure 4.4) (Carter, 1996):

1. Idealisation
2. Discretisation
3. Node and element numbering

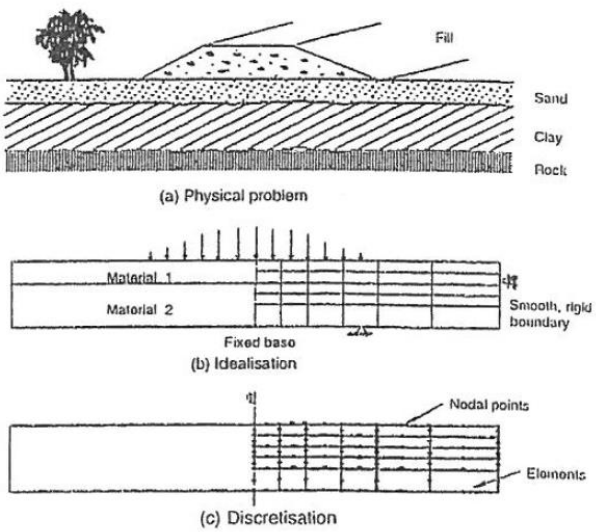

Figure 4.4: Modelling the physical problem. (Carter, 1996)

The idealization is achieved by breaking down the physical problem into its component parts (continuum components such as elastic regions) (Carter, 1996). Then the constitutive models have to be determined (Carter, 1996). Too much detailed model may clutter the analysis, the adequate level of

detail requires experience (Carter, 1996). The idealised model is then discretised using appropriate finite elements (Carter, 1996). Finally, node and element numbers are assigned. (Carter, 1996)

In geotechnical engineering, and geological strata modelling in particular, the numerical models divide the rock mass in elements (Wyllie and Mah, 2005). Each element is assigned a material model and properties (Wyllie and Mah, 2005). The material models or constitutive models represent the idealised stress/strain relation that describe how the material behaves, e.g. Mohr-Couloumb, Hoek-Brown, etc. (Wyllie and Mah, 2005). If the elements are connected together, the model is continuum, if they are separated by discontinuities, it is a discontinuum model (Wyllie and Mah, 2005). Discontinuum models allow slip and separation at explicitly located surfaces within the model (Wyllie and Mah, 2005). Although discontinuum methods allow slip, the product *RS2* (previously known as *Phase2*) of *Rocscience* which is a FEM program has the possibility of modelling a discontinuity (joint) and allows slip (Rocscience). An advantage of numerical modelling, which is absent in limit equilibrium methods, is that it not only gives the safety factor, but also the state of each element can be examined.

The current study is modelled in the following way. For the case of wedge sliding in a two-dimensional FEM program, the slip surface is designed with the trend and plunge of the intesection line of the two joint planes (see Chapter 4.2 - first scheme of presenting the wedge). The geometry of the model includes the slope and the embankment. The length of the slope is not considered in 2-dimensional modelling. The material properties are assigned from Table 2 and Table 5. The friction angle of the joint is 40°. The material model assigned is Mohr-Coulomb, the rock being with elastic behavior and the embankment being plastic type of material. The mesh is uniform made of 3-noded triangular elements. The boundary conditions are prescribed-displacement with restrained vertical and horizontal movement at the bottom of the model and restrained horizontal movement on the sides. The main model of the slope is created (Figure 4.5) and the from here on different analysis are performed.

With respect to the dynamic analysis, the FEM program *RS2* does not allow two pairs of damping coefficients for each material, so two separate models are created. To determine the Rayleigh damping coefficients of each model, the tutorial of the *Rocscience RS2* Manual “Dynamic Slope Analysis: Rayleigh Damping (Part C)” is followed. It includes natural frequencies analysis and setting the coefficients to the desired damping ratio.

To model the embankment and the rock structure as realistic as possible with their different damping properties, two FEM models are created – one presenting the railway embankment and one for the rock slope, since Rocscience *RS2* allows the user to input only one pair of damping coefficients for one model. With creating the first model of the embankment and applying the quasi-dynamic loading on it, the proper damping coefficients for the material are considered. At the bottom of the railway embankment, where it lies on the natural rock, the data for the ground vibration is extracted from a representative node and applied on the rock. The X velocity-time graph will be presented in the chapter for results, because it is a part of the work process and not a pre-defined influence.

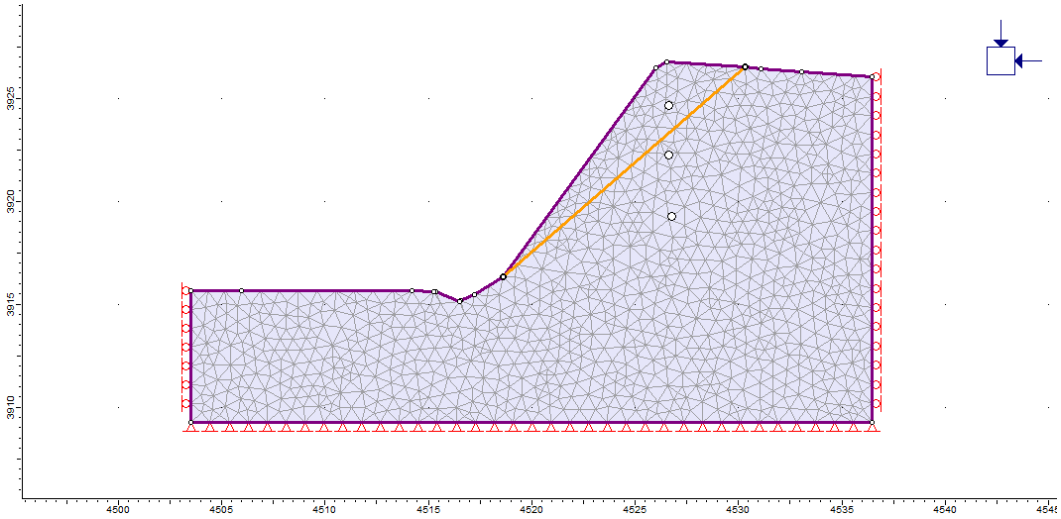

Figure 4.5: Modelling in RS2. The joints intersection line is represented by the orange line element. The boundary conditions are applied on the bottom and sides of the domain.

4.3.1. Static FEM analysis

Static analysis to estimate the slope stability safety factor are done with the Shear Strength Reduction method (SSR). The concept of the SSR approach is simple: systematically reduce the shear strength envelope of the material (Figure 4.6) by a factor of safety, and calculate finite element models of the slope until the deformations are unacceptably large or the solutions no longer converge (Rocscience, 2020).

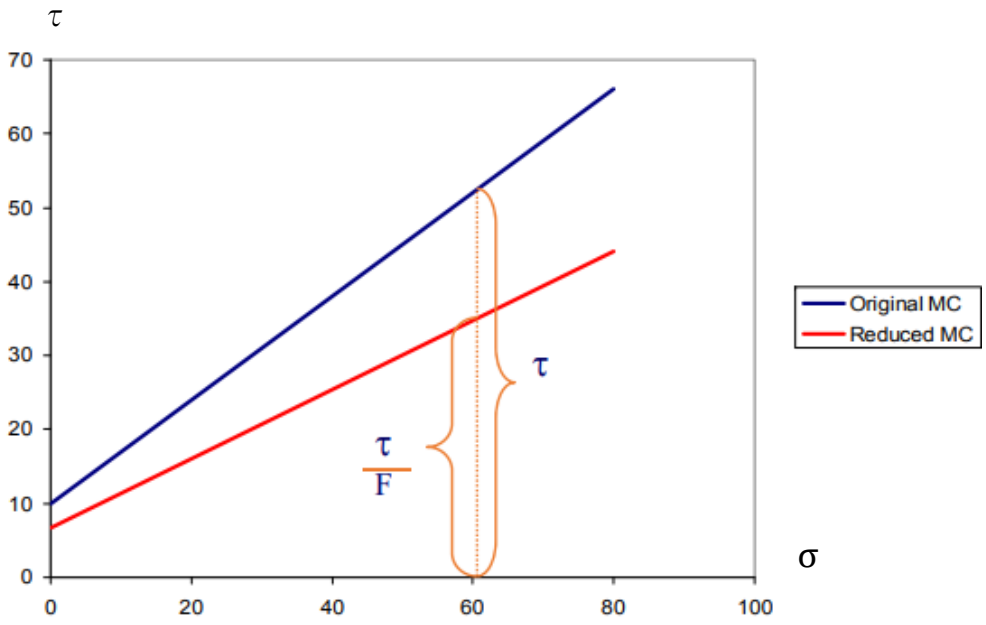

Figure 4.6: Shear Strength Reduction method for Mohr – Coulomb failure criterion. (Rocscience, 2020)

In the analyzes performed, the Mohr-Coulomb model was used for the geomaterials, in order to shape and reduce the shear strength envelope. The Mohr-Coulomb shear strength failure criterion assumes a linear relationship between shear strength in a plane and the normal force exerted on that plane and is expressed by:

$$\tau = c' + \sigma'.tg\varphi \qquad \text{Equation (14)}$$

where τ is the shear strength, σ' is the normal stress, φ is the internal friction angle and c' is the cohesion. This approach reduces the shear strength through a safety factor (FS), determined through the following equation (Rocscience, 2020):

$$\tau = \frac{c'}{FS} + \frac{\sigma' tg\varphi}{FS} \qquad \text{Equation (15)}$$

The factored Mohr – Coulomb properties after the application of SSR factor are (Rocscience, 2020):

$$c_{SSR} = \frac{c'}{FS}\ ,\ \varphi_{SSR} = arctg\left(\frac{tg\varphi}{FS}\right) \qquad \text{Equation (16)}$$

4.3.2. Dynamic FEM analysis

Dynamic analysis can be conducted by entering the dynamic influence and using Rayleigh damping. In RS2, dynamic loads can be applied to nodes. The loading data can be inputted in one of the four options: force, displacement, velocity, and acceleration. The data should be a set of time histories. The load types available in RS2 can be divided into external force loads and prescribed motion loads. The force type is applied to the model similar to static line loads and are essentially external forces that can vary over time and are applied at nodes. Such dependency is built according to the dimensions of the locomotive and wagons and the speed of the train composition (Figure 4.7).

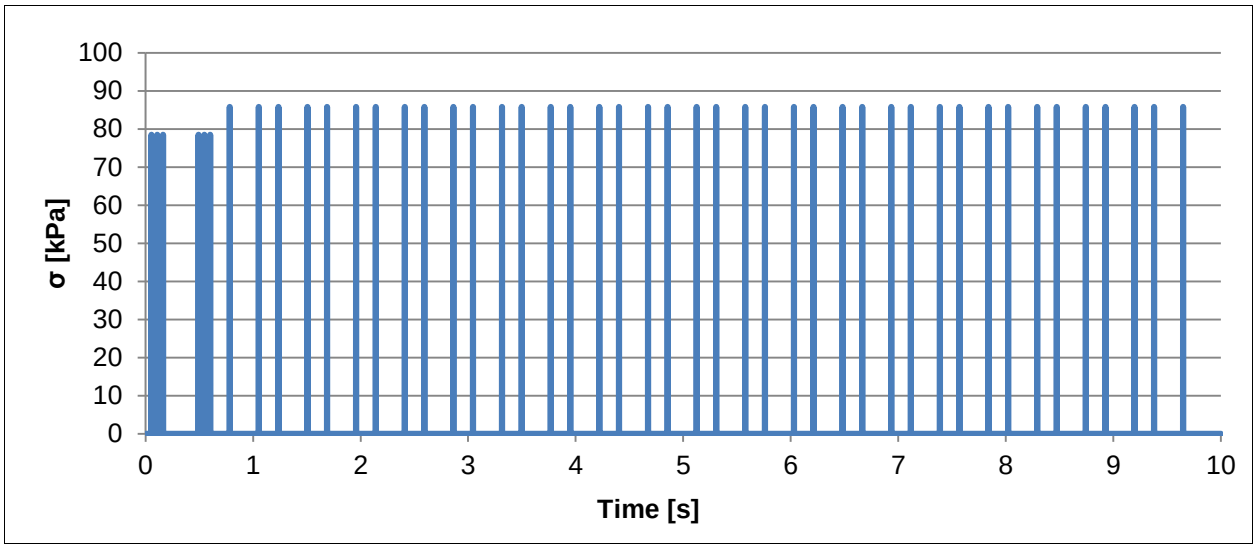

Figure 4.7: Time vs. distributed load induced by the passing of train with a speed of 120km/h, applied on the embankment.

The first 6 hights on the graph represent the influence of the 6 axles of the locomotive. The train composition is designed to travel with a speed of 120 km/h. By knowing the distances between the axles of the locomotive and the speed, the time for passing is calculated for each axle. The same was applied for the wagons and the graph of the passage of the train was built.

Displacement, velocity and acceleration loads are prescribed motion loads because they define the motion nodes during the dynamic simulation (Rocscience, 2020). The dynamic loading applied in the current model, is devided into two models in order to enter two different damping modes. The quasi-dynamic load-time graph is applied on the embankment model as a distributed load (Figure 4.7). Data for the vibration induced by the load is extracted at the bottom of the embankment and applied on the second model of the rock as velocity time history.

Dynamic boundary condition is a set of constraints that represents the effect of the boundary. Six types of dynamic boundary conditions are available in RS2, which are absorb, transmit, damper, nodal mass, tied, and hydro mass. In this case, the absorb dynamic boundary condition is applied to the bottom and side edges of the model. Absorb boundary condition is an artificial boundary condition that attempts to reproduce the infinite boundary behavior of the soil medium. The absorb boundaries absorb incoming shear and pressure waves as if the model was not actually bounded. The boundary is constructed from two dampers on the outer boundary, one perpendicular and the other tangential to the contour orientation (Figure 4.8), whose damping coefficient is proportional to the wave velocities (Rocscience, 2020).

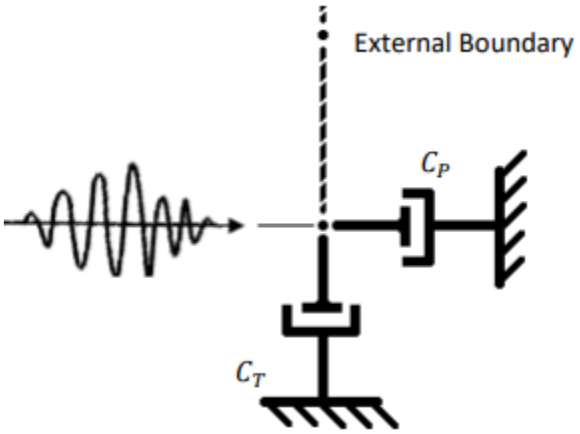

Figure 4.8: Dampers for Absorb Boundary Conditions (Rocscience, 2020).

For the factor of safety estimation in the conditions of dynamic influence, the Shear Strength Reduction method is applied again. Due to the limitation that the program has, that only dynamic or only SSR analysis can be performed at once, the SSR method is applied manually as it is suggested by Zhang et al. (2018) and Weidong Wu et al. (2019).

4.4. Comparison of methods used in the current and previous study

The study on the slope has started with kinematic analysis in both studies – the current study and Costa (2019), so they are identical in estimating the critical wedge prone to sliding.

The limit equilibrium method is applied more widely in the present study by calculating the safety factor using several formulas and using the product *SWedge*, while Costa (2019) uses only the program *SWedge*.

The main difference takes place in the 2D FEM modeling. There are two main aspects of modeling that change the simulations leading to uncomparable results. One of them is in defining the behaviour of the rock. Both models use the Mohr-Coulomb failure criterion, but in the current study the material is defined as elastic and in Costa, 2019 it is defined as plastic. The second aspect is the incorporation of the joints forming the wedge. In the previous study the two main joints are represented in the 2D model with their actual dip direction and dip. However, the program does not process the dip direction in 3D and assumes the joints are perpendicular to the cross-section that is being modeled. In the current study this disadvantage of the 2D modeling in *RS2* is taken into consideration and the joints were evaluated beforehand. Using the stereonet with stereographic projections of the joints, the line of intersection was estimated with its trend and plunge and then applied to the 2D model as one joint. In this way the wedge is presented as a planar sliding block, which is the disadvantage of modeling in two dimensions. By simulating the wedge in this way, it is able to slip on the joint (line of intersection).

5. Results

This chapter presents the results of analysing the slope with every method explained in the previous chapter and with every condition this study aims to discuss. The present study begins with the kinematic analysis of the joint system of the examined slope on the railway line of Beira Alta, Portugal. It is performed with the program *Dips*. Then the safety factor is calculated by formulas of force equilibrium (Eq. 7, 8, 9, 10, 12). Limit equilibrium method program *SWedge* is used for further calculations of the safety factor. Finite element method program *RS2* is used for static and dynamic analysis.

5.1. Kinematic analysis

The analysis carried out in *Dips* includes the stereographic projections of the groups of joints J1, J2, J3, J4, J5 and the projection of the slope face. The circle of the friction angle of the joints (40°) is drawn. The stereonet and the legend to it are displayed in Figure 5.1. The method of Markland is applied to determine the critical failures created by the joint planes. The lateral limit is set to 20°. There are no planar sliding and toppling failures estimated. The only critical block is a wedge created by joint groups J2 and J3. The Primary Critical Zone (highlighted in pink in the stereonet) for wedge sliding is the crescent shaped area inside the plane friction cone and outside the slope plane. Any intersection points that plot within this zone represent wedges which are able to slide. The Secondary Critical Zone (highlighted in yellow in the stereonet) is the area between the slope plane and a plane (great circle) inclined at the friction angle. Critical intersections which plot in these zones always represent wedges which slide on one joint plane. In this region, the intersections are actually inclined at less than the friction angle, but sliding can take place on a single joint plane which has a dip vector greater than the friction angle (Rocscience, 2020).

The intersection that falls into the Primary Critical Zone is of joint groups J2 and J3, so they are highlighted in dark red. No intersections fall in the Seconday Critical Zone. The joints that don't create critical blocks are projected in green colour (J1, J4, J5). The intersection line formed by joints J2 and J3 is projected as a point and from the stereonet the trend and plunge of the line are estimated to be 157°/41° (Figure 5.2). The kinematic analysis ends with the determination of the critical wedge.

The stereonet is also used to determine the angles ψ, β, ζ which are needed for further analyzes. The plunge of the intesection line ψ is estimated to be 41°. The angles ζ and β are measured on the blue arc which is connecting the poles of planes J2 and J3 (as shown on Figure 5.3). The measured angles are given in Table 6.

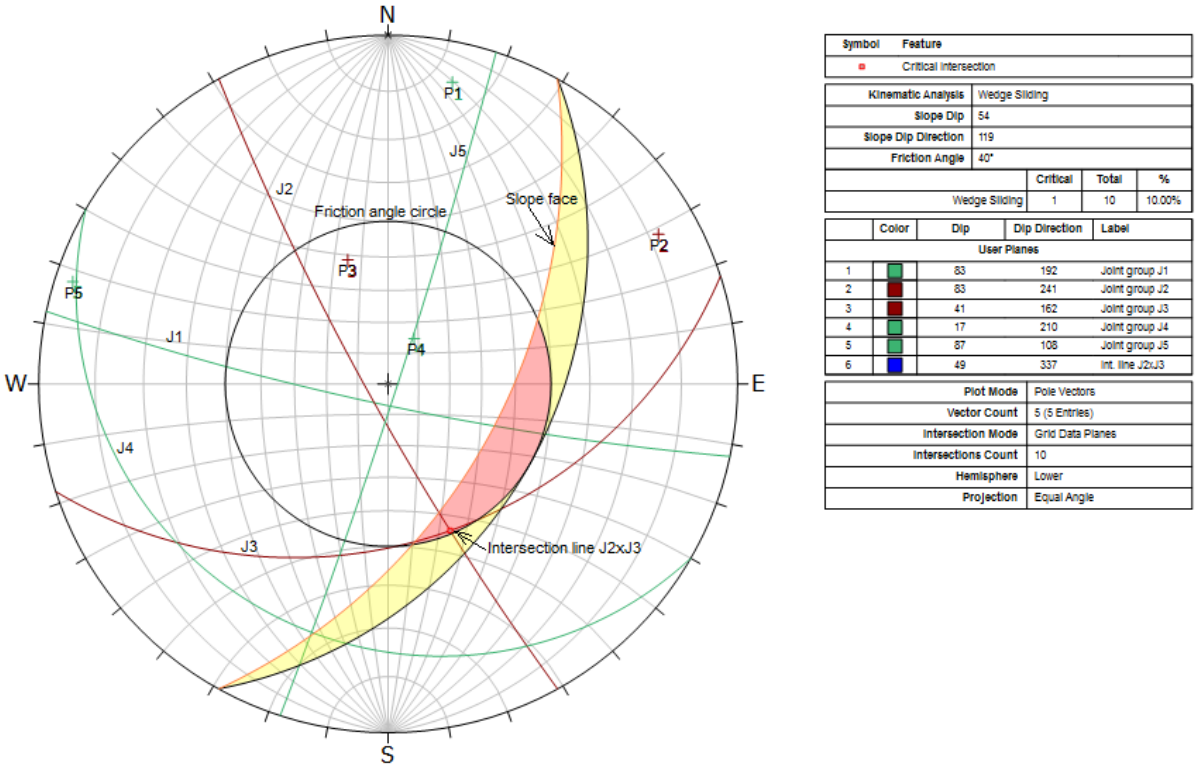

Symbol	Feature
	Critical Intersection

Kinematic Analysis	Wedge Sliding
Slope Dip	54
Slope Dip Direction	119
Friction Angle	40°

	Critical	Total	%
Wedge Sliding	1	10	10.00%

	Color	Dip	Dip Direction	Label
User Planes				
1		83	192	Joint group J1
2		83	241	Joint group J2
3		41	162	Joint group J3
4		17	210	Joint group J4
5		87	108	Joint group J5
6		49	337	Int. line J2xJ3

Plot Mode	Pole Vectors
Vector Count	5 (5 Entries)
Intersection Mode	Grid Data Planes
Intersections Count	10
Hemisphere	Lower
Projection	Equal Angle

Figure 5.1: Equal – angle streonet with projections of the slope face, the joint groups (J1,J2,J3,J4,J5), joint friction angle circle, joint poles (P1,P2,P3,P4,P5), the intersection line of J2 and J3.

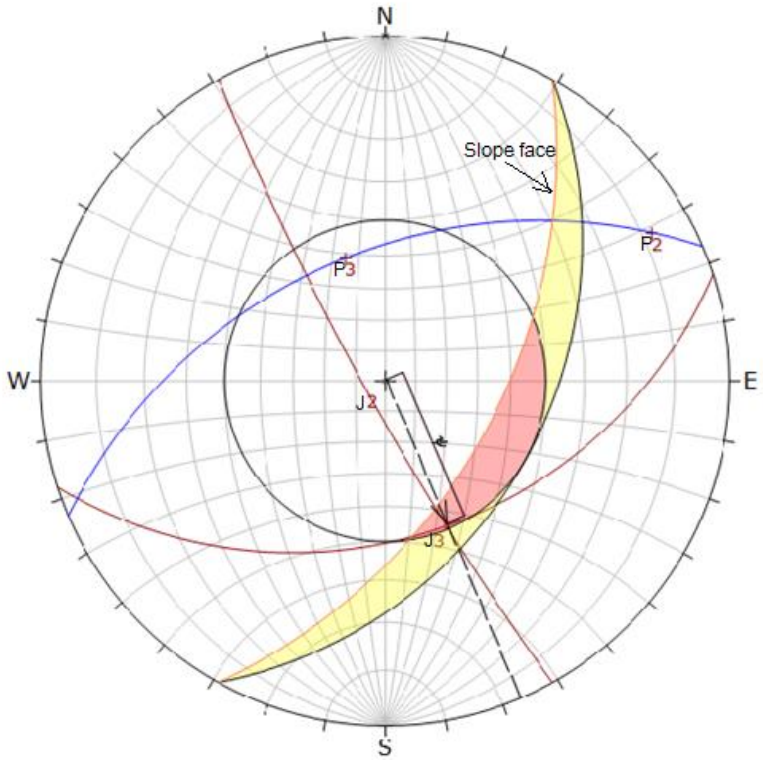

Figure 5.2: Estimation of trend and plunge of the line of intersection.

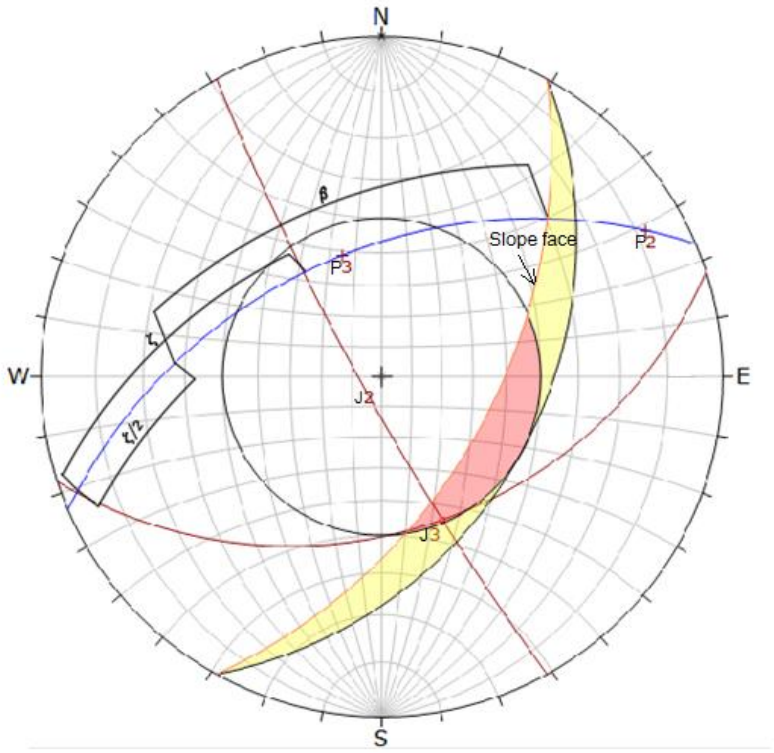

Figure 5.3: Estimation of angles β and ζ. The blue projection represents a fictional plane with a pole the intersection line J2xJ3.

Table 6: Measured angles from the stereonet.

Angle	Degrees
ψ	41°
β	100°
ζ	80°

5.2. Limit equilibrium analysis

The limit equilibrium analysis is performed by the two schemes mentioned above – firstly, the safety factor is calculated by Equation (7) as if planar sliding with orientation of the sliding surface as the one of the intersection line.

$$FS_1 = \frac{tg\varphi_{joint}}{tg\psi} = \frac{tg\ 40°}{tg\ 41°} = 0.97 \qquad \text{Equation (17)}$$

Secondly, the factor of safety is calculated as a wedge taking into consideration the 3-dimensional geometry of it by Equation 11.

$$FS_2 = \frac{sin\beta.tg\varphi_{joint}.tg\psi}{sin(\frac{\zeta}{2})} = \frac{sin100°.tg40°.tg41°}{sin\left(\frac{80}{2}\right)} = 1.12 \qquad \text{Equation (18)}$$

By the formula of Hoek et al. (1973) for friction-only calculation of safety factor in Equation (12), the coefficients A and B are estimated from the chart for dip difference between the two intersecting planes of 40° in Annex 1 as shown on Figure 5.4. Plane A is set to be J3 (162°/41°) and plane B is set to be J2 (241°/83°). The dip difference between them is 42° and the dip direction difference is 79°.

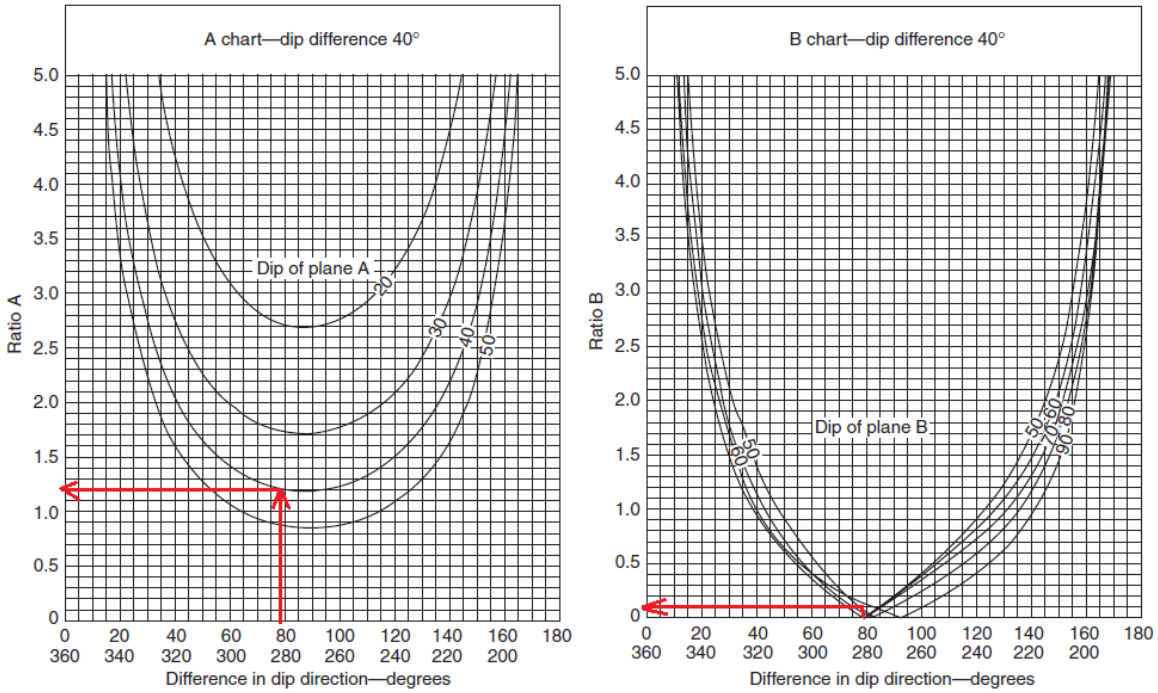

Figure 5.4: Estimation of coefficients A and B for friction-only calculation of stability safety factor of a wedge of Hoek et al. (1973).

The coeffiecients A and B are estimated and the safety factor is then calculated by Equation (12):

$$\mathrm{A} = 1.2$$

$$\mathrm{B} = 0.1$$

$$FS_3 = A.tg\varphi_A + B\ tg\varphi_B = 1.2.tg40° + 0.1.tg40° = 1.09 \quad \text{Equation (19)}$$

As mentioned in Chapter 4.2, if by this quick calculation the FS < 2.0, then further and more detailed analysis should be performed. The next assessment of the global stability under the current static conditions in carried out with the program *SWedge* (Figure 5.5) and the report from it is placed in Annex 2. The safety factor from *SWedge* is:

$$\mathrm{FS}_4 = 1.03$$

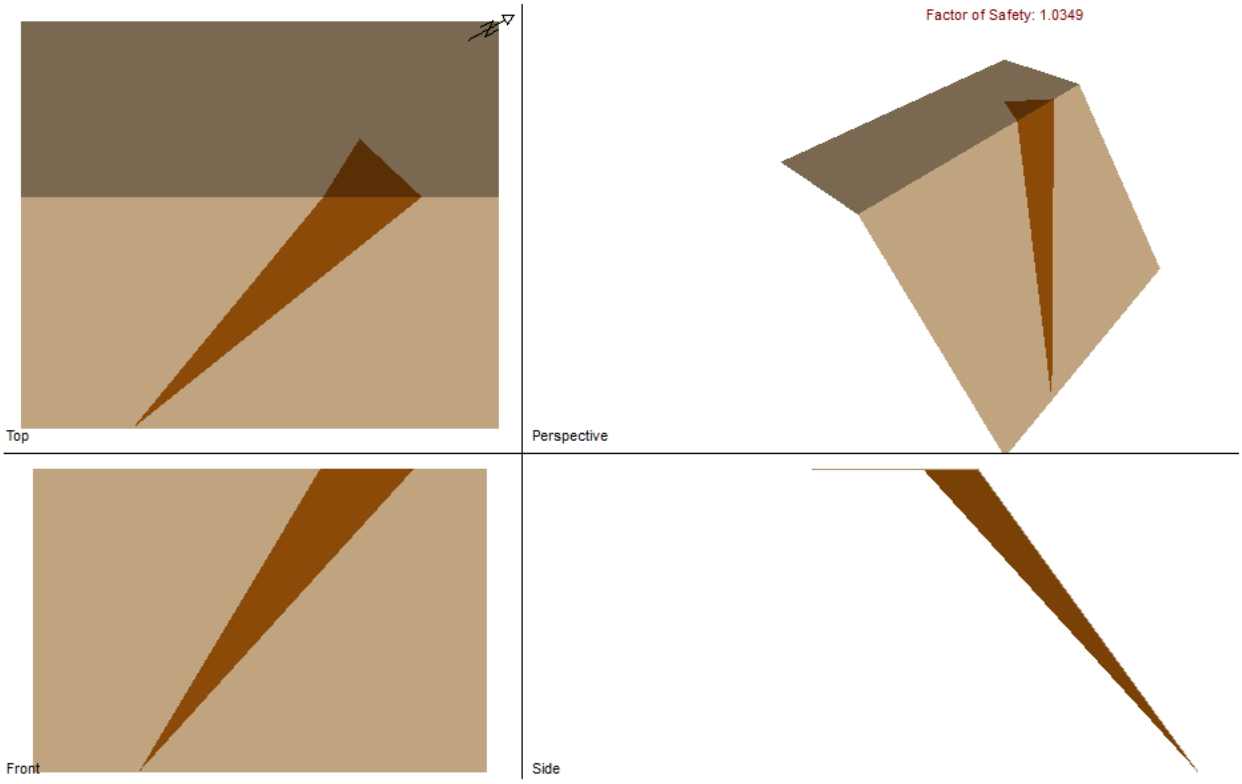

Figure 5.5: Analysis in *SWedge*.

5.3. Static FEM analysis

The static FEM analysis is performed in RS2 (2-dimensional), therefore the wedge stability is examined as planar block with slip surface represented by the intersection line of the two joint planes creating the wedge. The safety factor obtained from this analysis is:

$$\mathrm{FS}_5 = 0.96$$

The result from the SSR method is shown on Figure 5.6, where the green markers give the converged calculation and the red markers give the non-converged calculations. This means that with a SSR factor that gives a non-converged result, the block has detached and slipped.

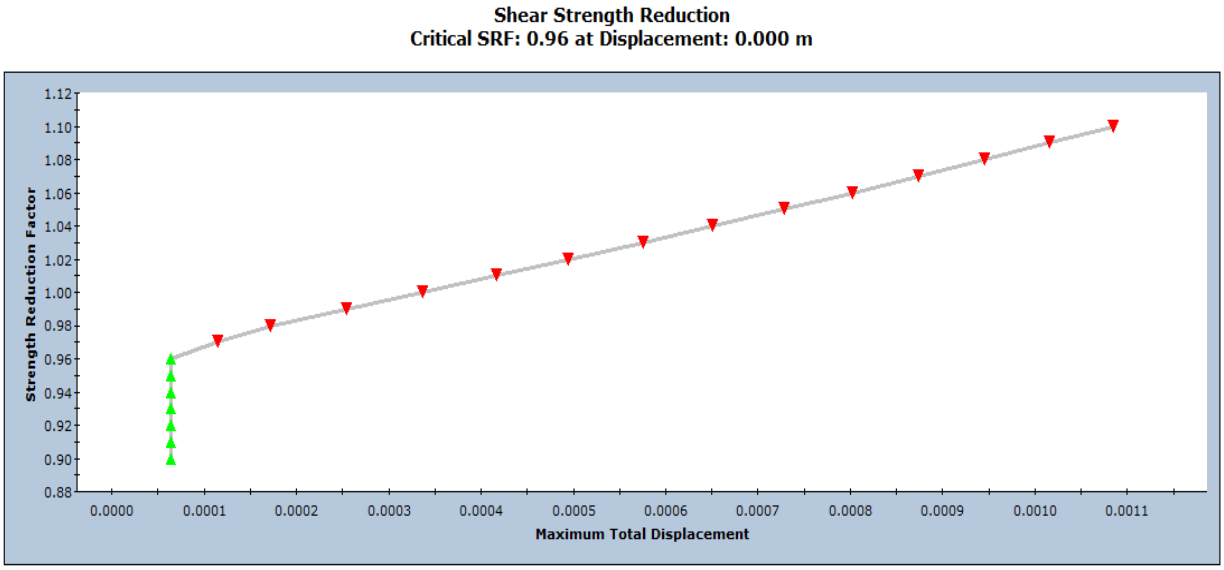

Figure 5.6: Shear Strength Reduction result applied for static analysis.

In Figure 5.7 is shown the development of the model with increasing the SSR factor from 0.96 to 0.97. The calculation at SSRF = 0.97 is the moment of detachment. It can be seen how at SSRF = 0.96 the maximum total displacement is still very little – 5.58e-07 m. At SSRF = 0.97 it drastically increases to 5.43e-05 m and as seen on Figure 5.6 keeps increasing with every higher SSR factor. After detachment and slipping the displacement is the same for the whole block.

a.

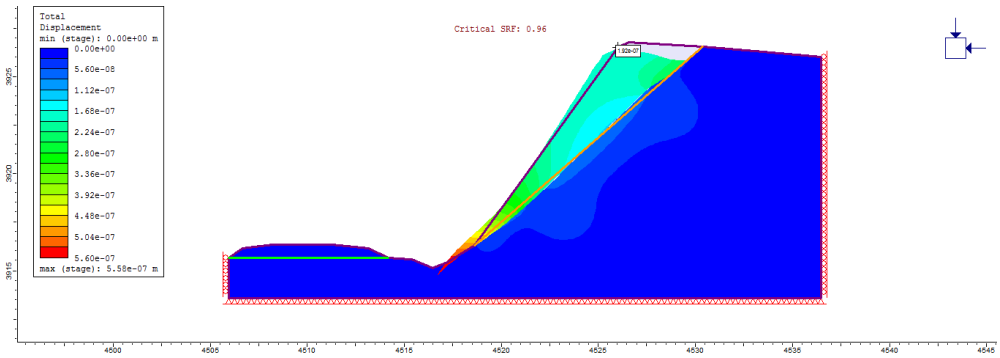

b.

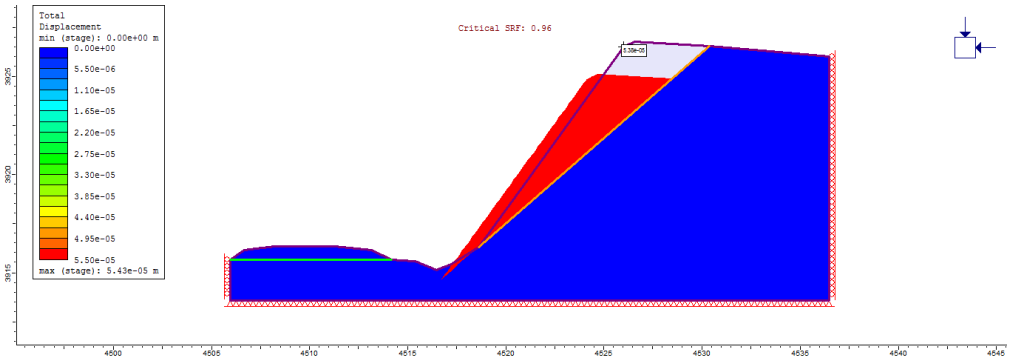

Figure 5.7: a. Shear Strength Reduction Model at SSRF=0.96; b. Shear Strength Reduction Model at SSRF=0.97.

5.4. Dynamic FEM analysis

There are two limitations of *RS2* in dynamic analysis found during the work. Firstly, the damping of the system is defined by Rayleigh coefficients α_M and β_K. The limitation comes from the fact that only one pair of coefficients can be inserted, while the damping of the different materials is different. Because of that, the dynamic analysis is broken down into two models – one of the embankment and one of the rock. The model of the embankment is subjected to the distributed load from the train passing with a speed of 120 km/h as shown on Figure 5.8.

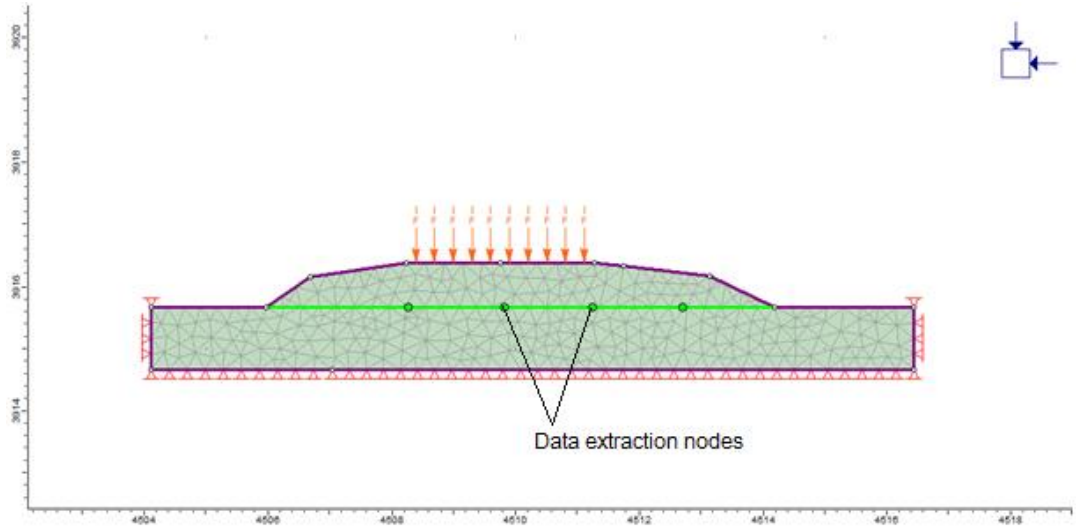

Figure 5.8: Embankment modelling with loading represented by the orange arrows acting on the surface. The green line represents the bottom of the embankment and the green points are nodes at which data of the ground vibration is extracted.

To estimate the Rayleigh damping coefficients in the program the following procedure is performed:

1. The model is computed undamped ($\alpha_M = 0$; $\beta_K = 0$) with the loading from the train passage.
2. At a typical node, data is collected for the X velocity – time history.
3. The tool *Dynamic data analysis* in the program is used. The velocity-time history is input and frequency-power graph is built.
4. The tool *Compute Natural Frequencies* is used which requires min and max frequency, in this case – 1 Hz and 100 Hz.
5. The coefficients are set to reach the desired damping ratio (Figure 5.9).

The damping ratio chosen for the estimation of the coefficients is defined by the maximum strain generated by the loading (Figure 5.10). The maximum strain is in the range of 0.02-0.07 and according to the damping curve for sand on Figure 2.5, the damping ratio is $\zeta = 4\%$.

Having the desired damping ratio, the Rayleigh coefficients are manipulated manually in the analysis shown on Figure 5.9 until aquired the average damping of 4%. The Rayleigh coefficients for the embankment are defined to be:

$$\alpha_M = 1$$

$$\beta_K = 0.0002$$

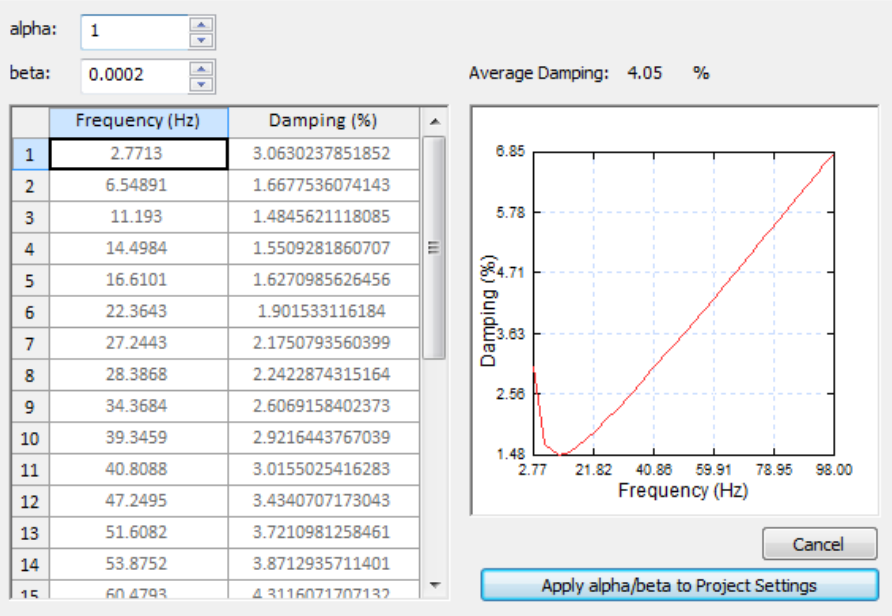

Figure 5.9: Natural Frequency Result - α_M and β_K estimation.

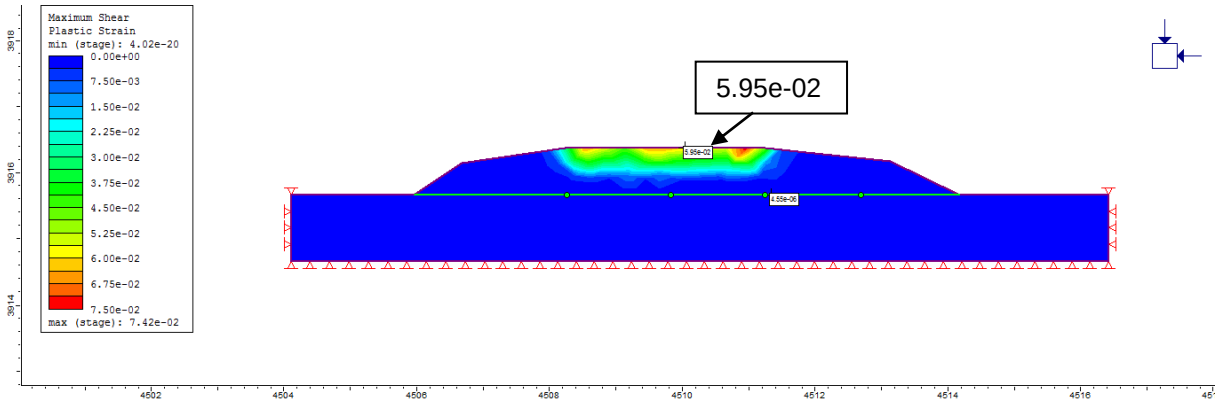

Figure 5.10: Maximum shear strain generated by the loading of the train passage.

After setting the damping coefficients, the model is computed and the data at the bottom of the embankment (data extraction nodes – Figure 5.8) is extracted as velocity-time history to be applied on the rock model (Figure 5.11).

The same procedure explained above is repeated for the rock model to estimate the damping coefficients. The strain of the rock is in the order of 1e-06, so according to the damping curve for rock (Schnabel et al., 1973) the damping ratio is ζ = 0.5%. The coefficients are set as:

$$\alpha_M = 0.1$$

$$\beta_K = 0.000012$$

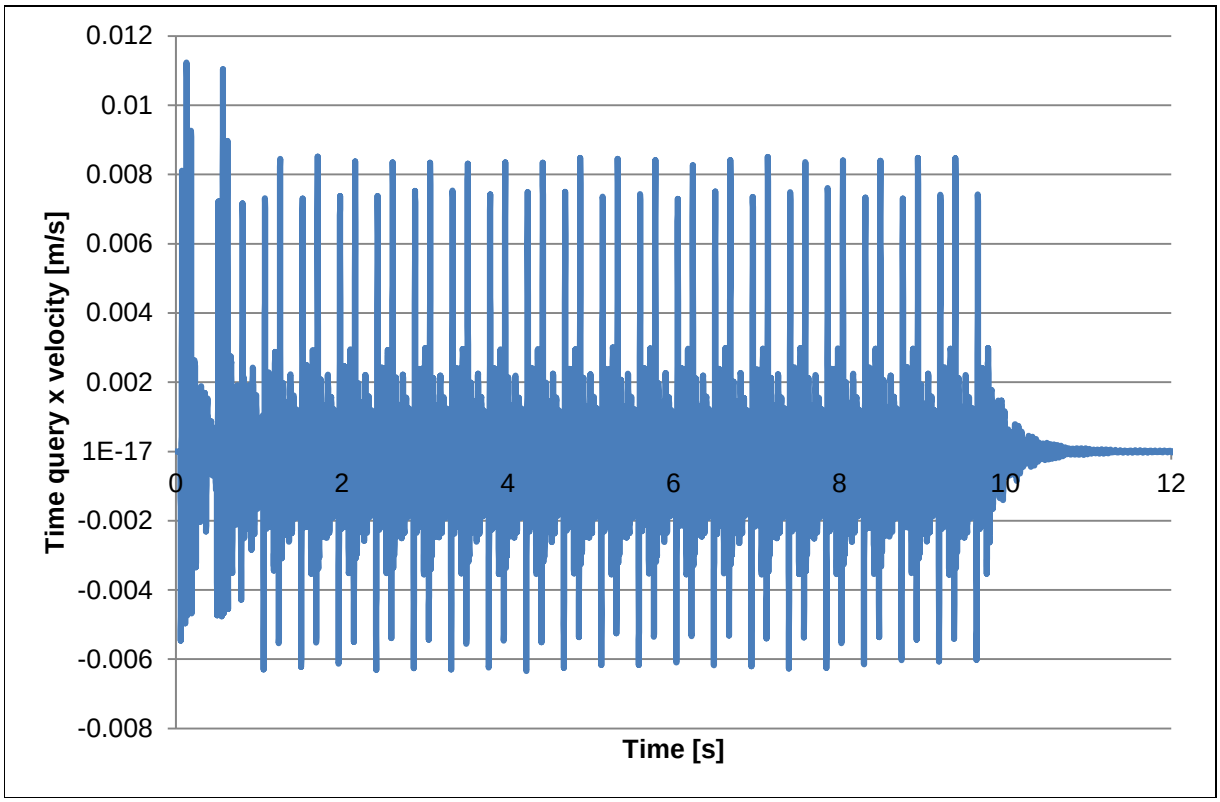

Figure 5.11: Time vs. X velocity of the ground vibration induced by the train traffic extracted at the bottom of the embankment from the embankment model.

Secondly, dynamic analysis and SSR analysis cannot work together at the same time. So, in order to obtain a slope stability safety factor the SSR method has to be applied manually. This process requires time for computing all the models. The friction angle of the slip surface is being reduced because the failure of a rock block depends on the joint properties. The joint friction angle is calculated with several SSR factors (Table 7) and the model is computed for each to obtain the maximum displacement. A graph giving the relation between SSR factor and maximum total displacement is built (Figure 5.12) and from which the slope stability factor of safety is determined.

Table 7: Joint friction angle values for SSR factors.

SSR factor	Friction angle, °
0.65	52.24
0.70	50.16
0.75	48.21
0.80	46.37
0.82	45.66
0.84	44.97
0.86	44.30
0.88	43.64
0.90	42.99
0.91	42.68
0.92	42.37
0.93	42.06
0.94	41.75
0.95	41.45
0.96	41.16
0.97	40.86
1.00	40

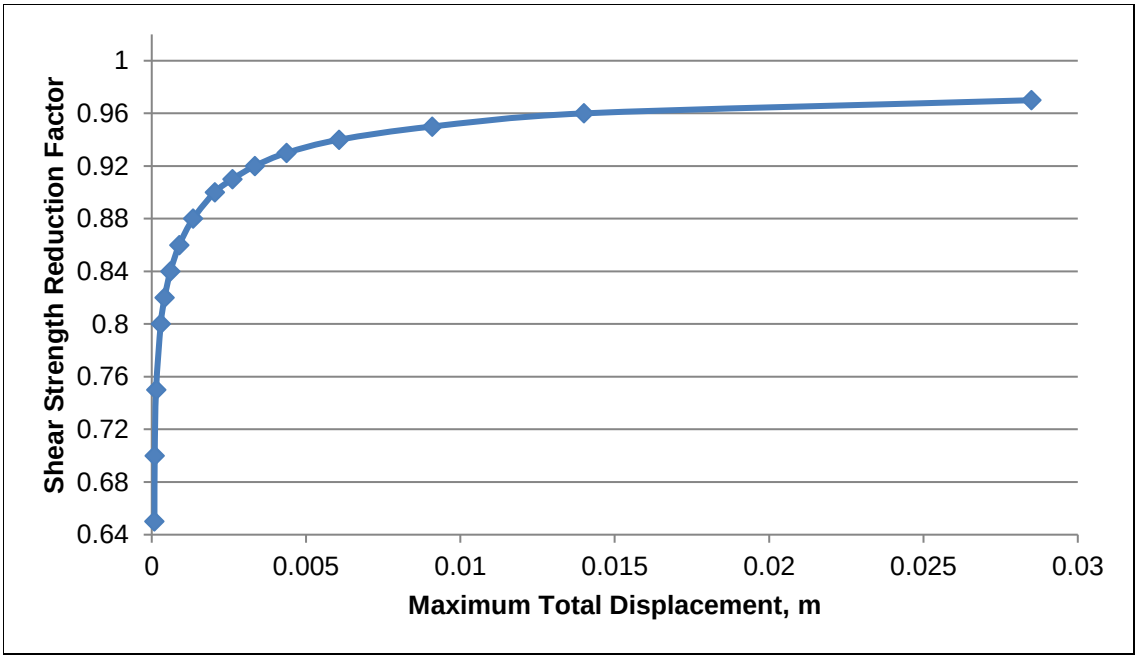

Figure 5.12: Shear Strength Reduction result applied for dynamic analysis.

The factor of safety is determined from the graph at the point where the displacement starts increasing progressively:

$$FS_6 = 0.86$$

5.5. Ground vibration mitigation measure

The mitigation measure chosen to limit the ground vibrations induced by the train is building a trench between the railway and the slope. Several depths of the trench are examined to determine the optimal depth. The horizontal and the vertical maximum vibration velocities at the 10th second of the passage of the train are used to understand the effect of the trench and its depth (Figures 5.13 and 5.14). The data is extracted at 2 nodes – Point A is right behind the trench barrier and Point B is inside the wedge body as shown on Figure 5.15.

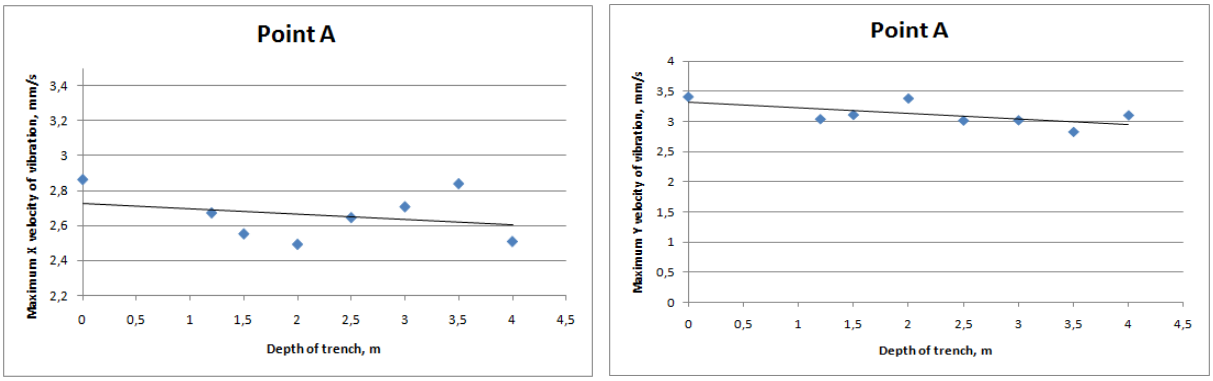

Figure 5.13: Maximum horizontal (left) and max vertical (right) velocities vs. depth of trench graphs at point A.

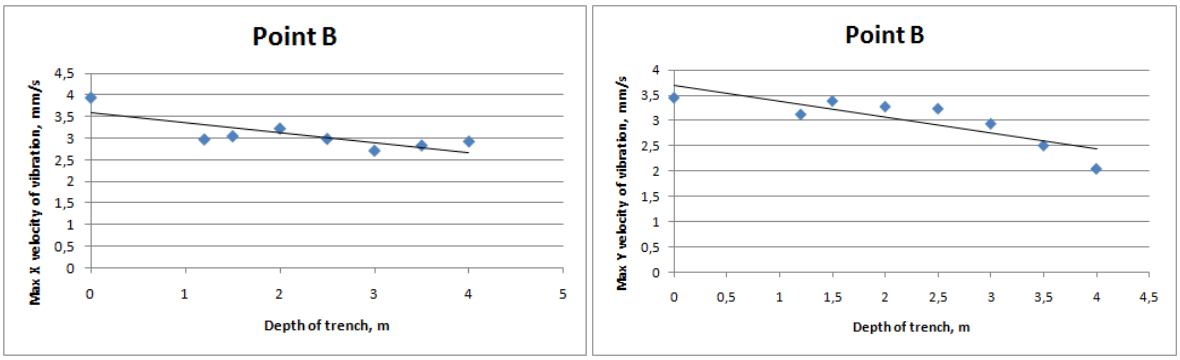

Figure 5.14: Maximum horizontal (left) and vertical (right) velocities vs. depth of trench graphs at point B.

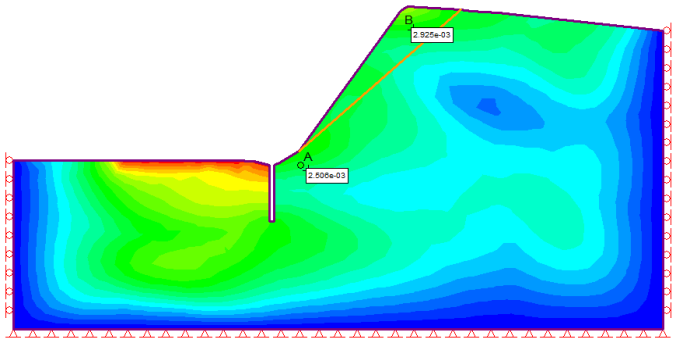

Figure 5.15: Representation of points A and B on the model.

The trendlines of all graphs shown above are slightly going down, which shows that with increase of the trench depth the vibration velocity decreases. However, with modeling of trenches deeper than 4 m the vibration velocity started to increase and the mitigation measure made the opposite effect.

The effect of the trench is examined by vibration reduction calculated for each depth of the trench (Figure 5.16). The horizontal component of the vibration velocity can be reduced up to 30% and the vertical – up to 40%.

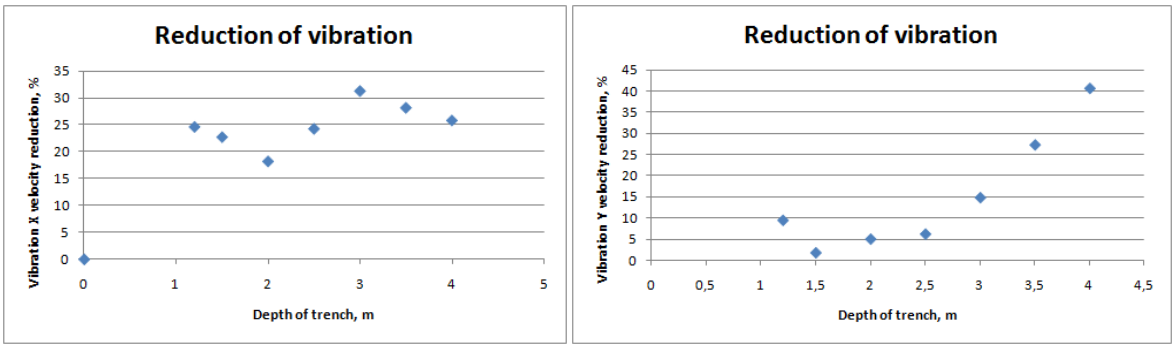

Figure 5.16: Reduction of horizontal (left) and vertical (right) ground vibration velocity at point B

After introducing the open trench barrier to mitigate the ground vibrations induced by the train traffic it is observed increase of ground vibration velocity at the face of the barrier as seen on Figure 5.17. This fenomena has been observed by Dinis da Gama and Paneiro (2006) and is due to the reflection and refraction of the seismic wave on the barrier.

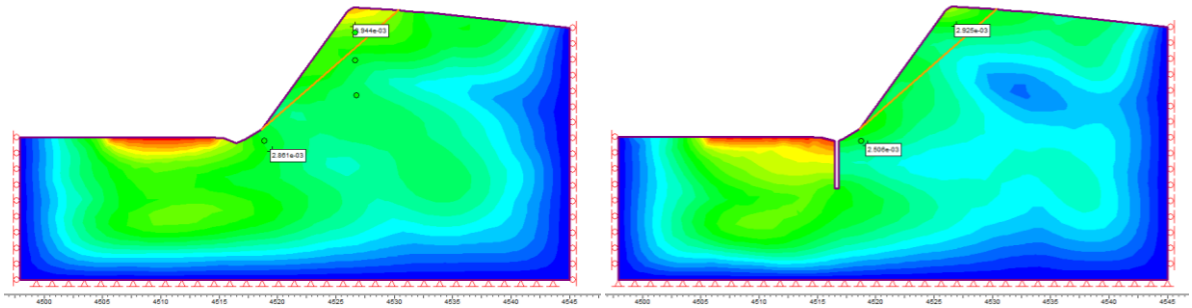

Figure 5.17: Ground vibration velocity induced by train traffic without (left) and with (right) an open trench barrier.

5.6. Static analysis results discussion

The slope stability safety factor is analysed using limit equilibrium method and finite element method. The results are summerised in Table 8.

Table 8: Static analysis FS results.

Method	Result for Factor of Safety
Planar sliding formula	$FS_1 = 0.97$
Wedge sliding formula	$FS_2 = 1.12$
Hoek et al. (1973) friction-only formula	$FS_3 = 1.09$
SWedge	$FS_4 = 1.03$
RS2	$FS_5 = 0.96$

From the results it can be observed that the analyzes that adopt a 2-dimensional scheme of calculation, assuming the wedge as a planar block with sliding surface orientation the one of the intersecting line of the wedge, have lower result for the factor of safety. The analyzes that take into consideration the geometry of the wedge as a 3-dimensional block are more detailed and accurate because of that reason. They give a higher value of the safety factor. However, the 2-dimensional analyzes give acceptable results in favor of security. From the results, it can be concluded that the block is in near the limit state and external or internal influences could lead to instability.

5.7. Dynamic analysis results discussion

Having the two limitations from the program – unable to input two different damping properties of the materials and unable to perform Shear Strength Reduction analysis paralel with the Dynamic analysis, the modelling and computing becomes a more complicated and time-consuming process. Compared to the static FEM analysis result, the safety factor obtained from the dynamic analysis with train-induced ground vibrations is obviously lower. This indicates that the train passage influences the stability of the slopes in the vicinity of the railway track.

Building a trench between the railway track and the slope is chosen for a mitigation measure. The depth of the trench is analyzed as a factor in limiting the vibrations induced by train traffic. At the moment after the passage of the train the trench helps the vibration to be reduced by 30% in horizontal direction and by up to 40% in vertical direction. Compared to other studies (Woods, 1968) which achieve vibration reduction of 75%, the current study does not give such results for vibration reduction by excavating a free barrier. One reason for this is the geological strata, which has lower damping properties.

5.8. Comparison of results from the current and previous study

The kinematic analysis made in both studies defines the critical wedge in the same way, using the same data for the joint groups. In the current study the stereographic net is used to define the orientation of the intersection line of the two joints forming the wedge.

The results from SWedge for limit equilibrium analysis also give the same result with the difference that in Costa (2019) the slope is examined with water pressure in the joints which decreases the safety factor. The safety factor without groundwater is FS = 1.03 and with joint water pressure is FS = 0.99. Additionally, in the current study the stability of the rock wedge is calculated by several formulas to compare the results and estimate the state of the critical block.

Considering the FEM analysis – static and dynamic – the comparison of results is debatable. The difference comes from the way of building the model of the slope, which was explained in the methodology comparison. The static safety factors are as follows:

- Costa (2019): FS = 1.02,
- the present study: FS = 0.96.

Both results are near the limit state. As seen on Figure 5.18 the failure mechanism which appears in the analysis of Costa (2019) is near-rotational failure. In the current study the failure mechanism is wedge sliding transformed to planar sliding due to the limitation of the 2D modeling. The block is designed to slip on the predefined joint.

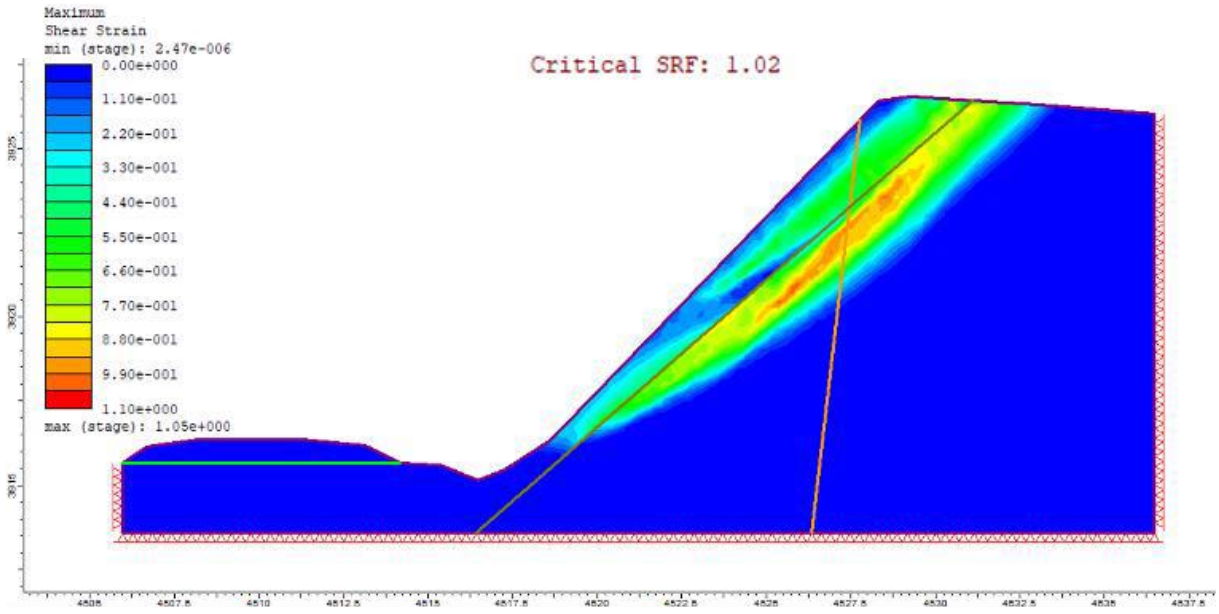

Figure 5.18: Static slope stability analysis from Costa, 2019.

When it comes to the dynamic analysis, there are several differences in modeling the dynamic load and the damping properties of the materials. Costa (2019) represents the dynamic load as a concentrated point load vs. time graph in the middle on the surface of the embankment. The damping properties of the materials are set the same for the whole model since the program doesn't allow a second pair of damping coefficients. In the current study the dynamic load is simulated as distributed load vs. time graph acting on the surface of the embankment with the width of the sleepers. The

damping properties are applied separately creating two models for each material. The results from the dynamic simulations are as follows:

- Costa (2019): FS = 0.57
- current study: FS = 0.86

The current study models the wedge in a whole different way, so the results are hard to compare. However, both show instability and influence from the passage of the train with the decrease of the stability safety factor.

6. Conclusions and future work

6.1. Conclusions

The goals set in the beginning of this paper are met after analyzing the study case, the specifics of the problem and after conducting several calculations according to the methods chosen. The studied slope which is situated in the northeast of Mainland Portugal is built of weathered granite with a system of joints, so the methods used for evaluation of its stability are from the rock mechanics.

The static kinematic analysis helped to find the critical wedge and the orientation of the intersection line. Considering the limit equilibrium method and the FEM in 2-dimensional calculations, they give similar results of instability (FS_1 = 0.97; FS_5 = 0.96), while the limit equilibrium method formulas considering the wedge in 3 dimensions give results of stability (FS_2 = 1.12; FS_3 = 1.09; FS_4 = 1.03). The results show that the 3-dimensional calculations of the safety factor give higher values than the 2-dimensional approaches and that is because the 3D calculations consider the reaction of both planes of the wedge. Having these results, it can be concluded that the wedge is in a limit state.

In the dynamic analysis, when compared to the static, it appears that the dynamic safety factor is lower that the static (FS_6 = 0.86), therefore, it can be concluded that there is influence of the railway-induced vibrations on the rock slope stability. The mitigation measure chosen to be applied and analyzed is a trench barrier between the railway track and the slope. At the last seconds of the passage the vibration velocity decreased by 30% in horizontal direction and up to 40% in vertical direction.

6.2. Future work

The current problem could be developed in direction of improving the input data of the dynamic influence by having geophysical tests to record the vibrations. A 3-dimensional FEM model can be made which will represent the actual geometry of the slope and wedge and probably would give more accurate results of the stability of the critical block. The 3-dimensional modelling can be used for the trench to analyze better the influence of it on vibration reduction. The slope can be examined with several trains passing during the day, as the traffic is not limited to one train.

References

Anbazhagan, P., Parihar, A. (2015). Selection of Modulus and Damping Curves for Site Response Study. *6th International Geotechnical Symposium on Disaster Mitigation in Special Geoenvironmental Conditions Chennai, India, January 21-23, 2015, Pages 161-164.*

Alzawi, A., Hesham El Naggar (2010). Full scale experimental study on vibration scattering using open and in-filled (GeoFoam) wave barriers. *Soil Dynamics and Earthquake Engineering, Volume 31, Issue 3, Pages 306-317.* doi:10.1016/j.soildyn.2010.08.010

Bandis, S., Lumsden, A.C., Barton, N.R. (1981). Experimental studies of scale effects on the shear behaviour of rock joints*. International Journal of Rock Mechanics and Mining Sciences & Geomechanics Abstracts, Vol.18, Issue 1, Pages 1-21.* doi:10.1016/0148-9062(81)90262-X

Barton, N. and Choubey, V. (1977): The Shear Strength of Rock Joints in Theory and Practice. *Rock Mechanics, 10, p.1-65.* doi:10.1007/BF01261801

Bulgarian National Railways – BDZ.

Carter, J. (1996). Numerical Methods in Geotechnical Engineering - From Research to Practice. *7th Australia - New Zealand Conference on Geomechanics (Adelaide, 1996).*

Caughey, T.K. (1960). Classical Normal Modes in Damped Linear Dynamic Systems. *Journal of Applied Mechanics Jun 1960, 27(2): 269-271*. doi:10.1115/1.3643949

Celebi, E., & Kırtel, O. (2013). Non-linear 2-D FE modeling for prediction of screening performance of thin-walled trench barriers in mitigation of train-induced ground vibrations. *Construction and Building Materials, 42, 122-131*. doi:10.1016/j.conbuildmat.2012.12.071

Connolly, D.P., Kouroussis, G, Laghrouche,O., Ho, C.L., Forde, M.C. (2015). Benchmarking railway vibrations – Track, vehicle, ground and building effects*. Construction and Building Materials 92 (2015), Pages 64–81.* doi:10.1016/j.conbuildmat.2014.07.042

Costa, A. (2019). Estabilidade de Taludes na Linha Férrea da Beira Alta Sob a Ação da Circulação Ferroviária.

CP Carga - Portuguese rail freight operator, Album de esquemas de vagões CP (2011).

Dinis da Gama, C., Paneiro, G. (2006). Minimization solutions for vibrations induced by underground train circulation. *11th ACUUS International Conference - Underground Space: Expanding the Frontiers, Athens.*

European Environment Agency report – term 2014: transport indicators tracking progress towards environmental targets in Europe. No.7/2014. doi:10.2800/857401

Geometrics, Inc. (2018), SeisImager/2D Seismic Refraction Data Analysis Software Manual and Examples Booklet.

Goktepe, F., Kuyuk, H.S., Celebi, E.(2014) Efficiency of wave impeding barrier in pipeline construction under earthquake excitation using nonlinear finite element analysis. *Sadhana-Academy Proceedings in Engineering Sciences, Volume 39, Pages 419–436*. doi:10.1007/s12046-014-0227-8

Hoek, E. and Bray, J. (1973). Rock Slope Engineering, *Inst. Mining and Metall, London*. ISBN 10: 0900488360

Hoek, E. and Bray, J.W. (1981) Rock Slope Engineering. Revised 3rd Edition, *The Institution of Mining and Metallurgy, London, 341-351.* ISBN-10: 0419160108

Hoek, E., Diederichs, M.S. (2006). Empirical Estimation of Rock Mass Modulus. *International Journal of Rock Mechanics and Mining Sciences, Volume 43, Pages 203-215.* doi:10.1016/j.ijrmms.2005.06.005

ISRM, Commission on Standardization of Laboratory and Field Test (1981a) Suggested Methods for the Rock Characterization, Testing and Monitoring, E.T. Brown (editor), *Pergamon Press, Oxford, UK, Page 211*. doi:10.1007/978-3-319-07713-0

Ji, S., Li, L., Motra, H. B., Wuttke, F., Sun, S.,Michibayashi, K., & Salisbury, M. H. (2018). Poisson's ratio and auxetic properties of natural rocks. *Journal of Geophysical Research: Solid Earth*, *Volume 123, Pages 1161–1185.* doi:10.1002/2017jb014606

Lines, L., Vasheghani, F. (2008). Reflections on Q. *CREWES Research Report*.

Liu, M., Gorman, D.G. (1995). Formulation of Rayleigh damping and its extensions. *Computers & Structures, Volume 57, Issue 2,1995, Pages 277-285*. https://doi.org/10.1016/0045-7949(94)00611-6

Markland, J. T. (1972) A useful technique for estimating the stability of rock slopes when the rigid wedge sliding type of failure is expected*. Imperial College Rock Mechanics Research Report No. 19,10pp.*

Medway– Transport and Logistics. Álbum Locomotivas. Série Euro 4000.

Mezeh, R. (2017). Advanced numerical modeling of vibrations induced by railway traffic.

Miller, G.H., Pursey, H. (1955). On the Partition of Energy between Elastic Waves in a Semi-Infinite Solid. *Proceedings of the Royal Society of London. Series A, Mathematical and Physical Sciences Vol. 233, No. 1192 (Dec. 6, 1955), Pages 55-69*. doi:10.1098/rspa.1955.0245

Mote, T., Morley, D., Keuscher, T, Crampton, T. (2004). GIS-based Kinematic Slope Stability Analysis.

Neves Ferro (1962). Carta Geològica de Portugal na escala de 1/50.000. Notìcia explicativa da folha 18-A Vila Franca das Naves, Lisboa, 1962.

Operational Program Transport and Transport Infrastructure (OPTTI 2014-2020).

Olivadoti, G. (2001). "Sensing, Analyzing, and Acting in the First Moments of an Earthquake." *Analog Dialogue*, *Vol. 35, January 2001*.

Paul de Vos, S. (2017). Railway induced vibration - State of the art report. *International Union Of railways*.

Rayleigh, L. (1885) On Waves Propagated along the Plane Surface of an Elastic Solid. *Proceedings of the London Mathematical Society, 17, Pages 4-11.* doi:10.1112/plms/s1-17.1.4

Rehnström, R., Widén, D. (2012). The influence of ballast on the vibrations of railway bridges.

Rocscience, RS2 User Manual (2020).

Rollins, K., Evans, M.D., Diehl, N.B., Daily, W.D. (1998). Shear modulus and damping relationships for gravels. *Journal of Geotechnical and Geoenvironmental Engineering Volume 126, Issue 12, Pages 1218-1218.*

Seed, H. B.; Idriss, I. M. (1970). Soil Moduli and Damping Factors for Dynamic Response Analyses. *EERC Report No.10-70, University of California*.

Schnabel, P. (1973). Effects of Local Geology and Distance from Source on Earthquake Ground Motions. PhD Thesis, *University of California, Berkeley, CA.*

Schwartz, A. E. (1964) Failure of rock in the triaxial shear test. *Proc. 6th Symp. on Rock Mech., Rolla, Missouri, Pages 109-151.*

Vàsàrhelyi, B. (2008). A possible method for estimating the Poisson's rate values of the rock masses. *Acta Geod. Geoph. Hung., Vol. 44(3), pp. 313–322*. doi:10.1556/AGeod.44.2009.3.4

Villeneuve, M. C., Heap, M. J., Kushnir, A. R. L., Qin, T., Baud, P., Guanglei Zhou, Tao Xu. (2018). Estimating in situ rock mass strength and elastic modulus of granite from the Soultz-sous-Forets geothermal reservoir (France). *Geotherm Energy 6:11*. doi.org/10.1186/s40517-018-0096-1

Wang, G. (2016). The Utilization of Slag in Civil Infrastructure Construction. Elsevier. ISBN: 978-0-08-100994-9

Weidong Wu et al., (2019). Two-dimensional dynamic analysis of seismic slope stability using DEM coupling with strength reduction technique. *IOP Conf. Ser.: Earth Environ. Sci. 304 042022*. doi:10.1088/1755-1315/304/4/042022

Woods, R. (1968). Screening of surface waves in soils. *Journal of the Soil Mechanics and Foundations Division, American Society of Civil Engineers, 94, Pages 951-979.*

Wyllie, D. C., Mah, C. W. (2005). Rock slope engineering: civil and mining — 4th edition. ISBN-10: 041528001X

Zerwer, A., Cascante, G., Hutchinso, J. (2002). Parameter Estimation in Finite Element Simulations of Rayleigh Waves. *Journal of Geotechnical and Geoenvironmental Engineering, March 2002, 250-261*. doi:10.1061/(ASCE)1090-0241(2002)128:3(250)

Zhang, H., Li, S., Zhang, X., Han, L., Ding, Z., Xu, C. (2018). Research on Method of Dynamic Stability Analysis for Slopes of Earth and Rockfill Dam Basing on the P-Z Model. *Technical Gazette 25, 1(2018), 230-235*. doi:10.17559/TV-20170322074315

Деянов, Д.(1993). Локомотивното стопанство на БДЖ 1947 – 1990, София.

Лаков, А. (2018). Устойчивост на скални откоси в условията на открити рудници и кариери – Автореферат на дисертация.

Annex 1

Wedge stability chart for friction only: A and B charts for a dip difference of 40°

The chart is used for estimation of the coefficients A and B for calculation of the stability safety factor of a wedge (Hoek et al., 1973) for a dip difference of 40° of the two joints cutting the wedge.

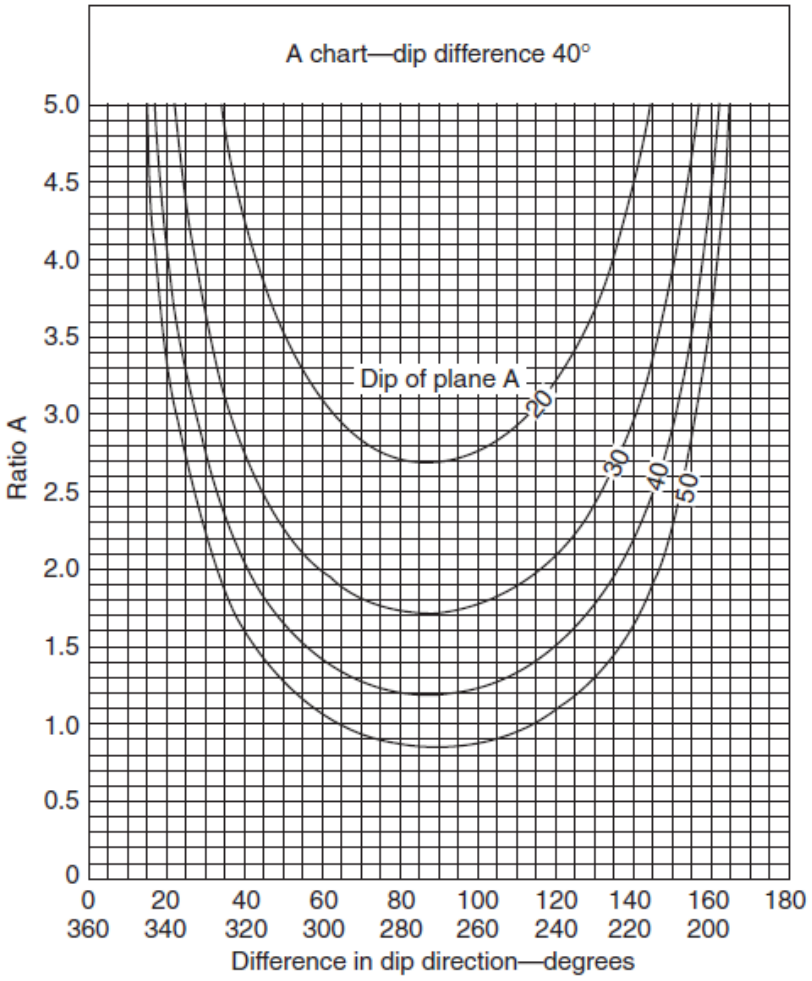
A chart—dip difference 40°
Ratio A
5.0
4.5
4.0
3.5
3.0
2.5
2.0
1.5
1.0
0.5
0
Dip of plane A
20
30
40
50
0 20 40 60 80 100 120 140 160 180
360 340 320 300 280 260 240 220 200
Difference in dip direction—degrees

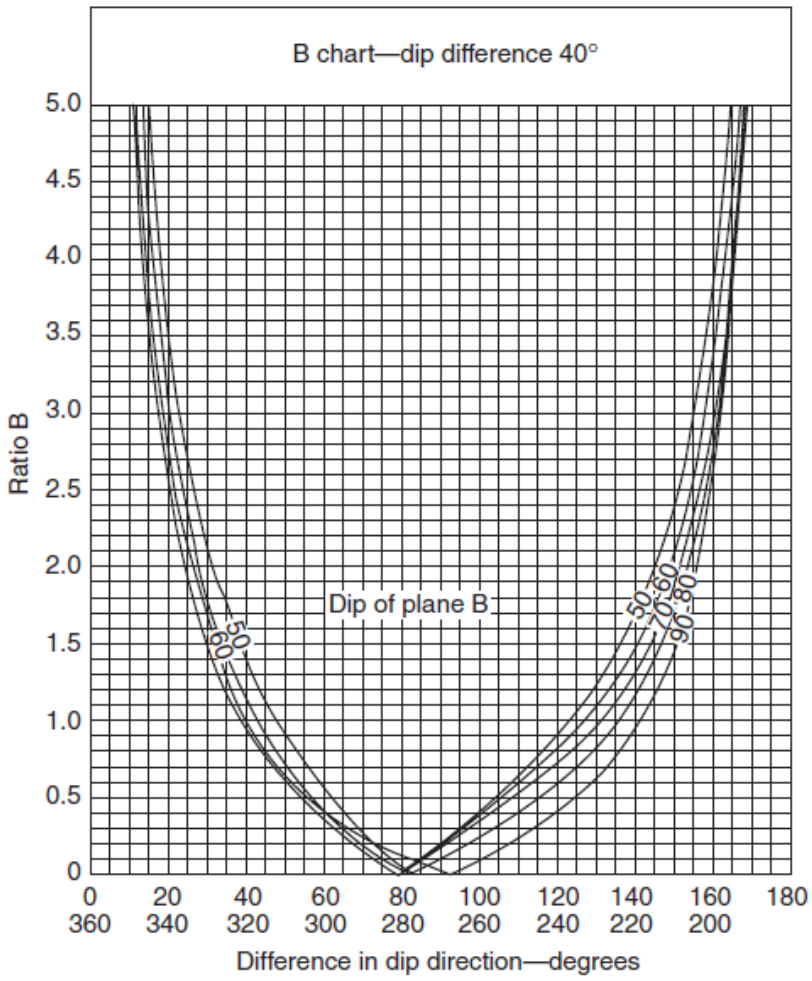
B chart—dip difference 40°
Ratio B
5.0
4.5
4.0
3.5
3.0
2.5
2.0
1.5
1.0
0.5
0
Dip of plane B
50-50
50-60
70-70
90-80
0 20 40 60 80 100 120 140 160 180
360 340 320 300 280 260 240 220 200
Difference in dip direction—degrees

Annex 2

Report from *SWedge* for Limit Equilibrium Analysis

To obtain a stability safety factor in the program *SWedge* the wedge is designed as follows. The wedge is built in the program with its actual dimensions – the dip and dip direction of the joints J2 and J3 that cut the block and of the slope face, height of 15 m. The properties of the rock are taken from Table 2. The friction angle of the joints id 40°.

Deterministic Analysis
Factor of Safety: 1.0349

Wedge Data
Volume: 31.616 m3
Weight: 853.628 kN
Area (joint1): 24.322 m2
Area (joint2): 45.756 m2
Area (slope face): 42.949 m2
Area (upper face): 6.323 m2
Normal Force (joint1): 37.000 kN
Normal Force (joint2): 652.242 kN
Normal Stress (joint1): 1.521 kPa
Normal Stress (joint2): 14.255 kPa
Shear Strength (joint1): 1.276 kPa
Shear Strength (joint2): 11.961 kPa
Driving Force: 558.864 kN
Resisting Force: 578.342 kN
Mode: Sliding on Joints 1&2

Sliding Direction
Plunge: 40.896 deg
Trend: 157.105 deg

Line of Intersection
Plunge: 40.896 deg
Trend: 157.105 deg
Length: 22.912 m

Slope Input Data
Height: 15.000 m
Dip: 54.000 deg
Dip Direction: 119.000 deg

Upper Face Input Data
Dip: 0.000 deg
Dip Direction: 119.000 deg

Joint1 Input Data
Dip: 83.000 deg
Dip Direction: 241.000 deg
Waviness: 0.000 deg
c: 0.000 kPa
Phi: 40.000 deg

Joint2 Input Data
Dip: 41.000 deg
Dip Direction: 162.000 deg
Waviness: 0.000 deg
c: 0.000 kPa
Phi: 40.000 deg

Trace Length
Joint1: 20.602 m
Joint2: 23.003 m

Persistence
Joint1: 22.912 m
Joint2: 23.003 m